

1 **Rhenium-osmium systematics and major and trace element chemistry of**  
2 **cobaltite (CoAsS): Evidence for Late Mesoproterozoic sediment-hosted Co-Cu**  
3 **sulfide mineralization with Grenvillian and Cretaceous remobilization in the**  
4 **Idaho Cobalt Belt, Belt-Purcell Basin, USA**

5

6

N. J. Saintilan<sup>1</sup>, R. A. Creaser<sup>1</sup>, A. A. Bookstrom<sup>2</sup>

7

8 <sup>1</sup>Department of Earth and Atmospheric Sciences, University of Alberta, Edmonton, Alberta, T6G  
9 2E3, Canada

10 <sup>2</sup>U.S. Geological Survey, 904 W. Riverside Avenue, Spokane, Washington 99201, USA

11

12

13 Corresponding author:

14 Nicolas J. Saintilan

15 [saintila@ualberta.ca](mailto:saintila@ualberta.ca)

16

## 17 **Abstract**

18 We report the first study of the Re-Os systematics of cobaltite (CoAsS) using disseminated and  
19 massively mineralized samples from two breccia-type and two stratabound deposits from the Co-Cu-Au  
20 Idaho Cobalt Belt, Lehmi Sub-basin to the Belt-Purcell Basin, Idaho, USA. Using a  $^{185}\text{Re}+^{190}\text{Os}$  spike  
21 solution, magnetic and non-magnetic fractions of cobaltite mineral separates give reproducible Re-Os  
22 analytical data for aliquot sizes of 150 to 200 mg. Cobaltite has highly radiogenic  $^{187}\text{Os}/^{188}\text{Os}$  (17–45)  
23 ratios and high  $^{187}\text{Re}/^{188}\text{Os}$  (600–1800) ratios but low Re and total Os contents of ca. 0.4–4 ppb and 14–64  
24 ppt, respectively. With proportions of radiogenic  $^{187}\text{Os}$  between 30 and 74%, cobaltite from the Idaho  
25 Cobalt Belt is amenable to Re-Os age determination using the isochron regression approach.

26 The Re-Os data for disseminated cobaltite mineralization in a quartz-tourmaline breccia from the  
27 Haynes-Stellite deposit yield a Model 1 isochron age of  $1349 \pm 76$  Ma ( $2\sigma$ ,  $n = 4$ , mean squared weighted  
28 deviation  $\text{MSWD} = 2.1$ , initial  $^{187}\text{Os}/^{188}\text{Os}$  ratio of  $4.7 \pm 2.2$ ). This middle Mesoproterozoic age  
29 information was preserved despite a possible phase of metamorphism or a pulse of metamorphic-  
30 hydrothermal remobilization of pre-existing cobaltite mineralization along fold cleavages during the  
31 Grenvillian orogeny. This phase of remobilization was tentatively identified through a Model 3 isochron  
32 age of  $1132 \pm 240$  Ma ( $2\sigma$ ,  $n = 7$ ,  $\text{MSWD} = 9.3$ , initial  $^{187}\text{Os}/^{188}\text{Os}$  ratio of  $9.0 \pm 2.9$ ) in the quartz-  
33 tourmaline breccia from the Idaho Zone.

34 Although all Mesoproterozoic cobaltite mineralization was subject to lower-upper greenschist to  
35 lower amphibolites in garnet zone metamorphism from Late Jurassic to Late Cretaceous during the  
36 Cordilleran orogeny in the Blackbird district, the fine- to coarse-grained massive cobaltite mineralization  
37 from the Chicago Zone is the only studied deposit that has severely disturbed Re-Os systematics with  
38 evidence for a linear trend of mixing with (metamorphic?) fluids in the  $^{187}\text{Os}/^{188}\text{Os}$  vs.  $1/^{192}\text{Os}$  space.  
39 Given the position of the Chicago Zone in the Blackbird metamorphic domain characterized by middle to  
40 upper greenschist metamorphism, and, the thermal conditions of Cretaceous metamorphism between 400  
41 and 520°C in the overlying garnet-bearing Indian Creek metamorphic domain, a maximum closing  
42 temperature of 400°C for the Re-Os isotopic system in cobaltite is proposed. In addition, our study

43 suggests that small, high-grade, structurally-controlled satellite deposits, which are located ca. 15 km to  
44 the SE of the Blackbird district (e.g., Black Pine), are product of Cretaceous remobilization of  
45 Mesoproterozoic cobaltite deposits in the Blackbird district.

46         The new Re-Os ages and the extremely high initial  $^{187}\text{Os}/^{188}\text{Os}$  ratios are in favor of a magmato-  
47 hydrothermal genetic model for a multi-stage REE-Y-Co-Cu-Au mineralization between ca. 1370 Ma and  
48 1349 Ma related to the emplacement of the Big Deer Creek granite at ca. 1377 Ma. Following deposition  
49 of paragenetically early xenotime, gadolinite and Be-minerals, a mixture of Mesoproterozoic evaporitic  
50 brines and magmatic fluids derived metals and reduced sulfur from mafic and oceanic island-arc Archean  
51 to Paleoproterozoic rocks from the Laurentian basement of the Great Falls Tectonic Zone. Cobaltite  
52 mineralization (and the closure of the Re-Os isotope system in this mineral) occurred upon cooling of  
53 these fluids at an inferred temperature of 300°C or below.

54

55 **Keywords** cobaltite, Re-Os, geochronology, Mesoproterozoic, metamorphism, greenschist, Idaho

56 Cobalt Belt, magmato-hydrothermal, xenotime, Great Falls tectonic zone

## 57 **1. Introduction**

58 Cobaltite –CoAsS–, which crystallizes in the orthorhombic system, belongs to the group of  
59 sulfarsenides along with gersdorffite (NiAsS, cubic) and arsenopyrite (FeAsS, monoclinic). Cobaltite is  
60 found in a variety of ore deposits, including mafic to ultramafic-hosted massive sulfide deposits (e.g.,  
61 Main Uralian Fault Zone, southern Urals; Nimis et al., 2008), orogenic gold deposits (e.g., Oberon gold  
62 prospect, Northern Territory, Australia; Cook et al., 2013; Huston et al., 2007; Tunks and Cooke, 2007;  
63 Loulo mining district, Mali; Lawrence et al., 2013; Otago and Alpine Schists, New Zealand; Pitcairn et al.,  
64 2006), and sediment-hosted Co-Cu deposits of the Idaho Cobalt Belt, Idaho, USA (cf. Bookstrom et al.,  
65 2016). Cobaltite is also known to crystallize with gersdorffite from immiscible sulfarsenide liquid from  
66 calc-alkaline magma (Beziat et al., 1996).

67 Other (sulf-)arsenides such as arsenopyrite and löllingite (FeAs<sub>2</sub>, orthorhombic) have been proven  
68 to be hosts for both rhenium (Re) and osmium (Os) with Re concentrations in the order of 10 to 1000s of  
69 ppb, and, Os concentrations in the 10-100s ppt range and up to the ppb level. The use of the Re-Os  
70 isotopic system in these minerals with isochron age determinations constrained the timing of gold  
71 mineralization in hydrothermal gold deposits (Mikulski et al., 2005; Davies et al., 2010; Morelli et al.,  
72 2010) and also brought new insights into the metamorphic evolution of the Broken Hill area in Australia  
73 (Saintilan et al., *accepted in Canadian Mineralogist*). Hence, these results and the similarity of crystalline  
74 structure between cobaltite and löllingite form a logical basis to investigate the Re-Os isotope system in  
75 cobaltite and evaluate the potential of this mineral for Re-Os age determination.

76 In this study, cobaltite was sampled from Co-Cu-Au deposits hosted by metasedimentary rocks of  
77 the Idaho Cobalt Belt, Idaho, USA (Fig. 1). This metallogenic province was chosen as the best example  
78 for which the parameters of basin stratigraphy, structural and tectonic features resulting from basin  
79 inversion, compressive tectonics and related metamorphic history are well-constrained by geologic and  
80 geochronological evidence (cf., Lund and Tysdal, 2007; Zirkparvar et al., 2007; Lund et al., 2011;  
81 Aleinikoff et al., 2012; Bookstrom et al., 2016). We chose to focus on the Haynes-Stellite deposit and the  
82 Chicago and Idaho Zones of the Blackbird mine, and the Black Pine deposit to the southeast of the

83 Blackbird area (Fig. 1B). However, no geochronological data exist on the Co- and Cu-rich sulfides in  
84 these deposits and both Proterozoic (Aleinikoff et al., 2012, Slack, 2012; Bookstrom et al., 2016) and  
85 Cretaceous (Lund et al., 2011) ages for mineralization have been proposed. The unresolved issue of the  
86 timing of mineralization feeds the debate on the genetic model for Co-Cu-Au mineralization in the Idaho  
87 Cobalt Belt (cf., Nold, 1990; Slack, 2006; Lund et al., 2011; Slack, 2012).

88         Herein, we carry out a two-fold Re-Os investigation of cobaltite mineralization: (1) to assess the  
89 degree of preservation of the Re-Os systematics of cobaltite in the four deposits through Cretaceous  
90 greenschist to lower amphibolites metamorphic overprint; (2) to determine if cobaltite mineralization is  
91 Proterozoic or Cretaceous in age for each of the deposits. Given the framework in which Re-Os isotope  
92 data can be assessed and interpreted further by using available geologic, petrographic and stable and  
93 radiogenic isotope data (Slack, 2006; Slack, 2012; Johnson et al., 2012; Panneerselvam et al., 2012;  
94 Bookstrom et al., 2016), the new Re-Os ages for cobaltite mineralization provide a better understanding of  
95 the origin of these deposits and the derived initial Os ratio further constrains the source of Os, and by  
96 inference, other metals like Co.

97

## 98 **2. Geologic background and chronostratigraphy of the Idaho cobalt belt**

99         The Idaho cobalt belt (ICB; Fig. 1), in the Salmon River Mountains of east-central Idaho, U.S.A.,  
100 is a northwest-trending belt of 45 known cobalt (Co) ± copper (Cu) ± gold (Au)-bearing mineral  
101 occurrences (Johnson et al., 1998). Mineralization is hosted by metasedimentary rocks of the Lemhi sub-  
102 basin in the southwestern part of the Mesoproterozoic Belt-Purcell basin, which is east of and inboard  
103 from the rifted continental margin (Fig. 1A). The rocks of the western Belt-Purcell basin underwent  
104 regional metamorphism during the Middle to Late Mesoproterozoic (Ectasian and Stenian) and the  
105 Jurassic–Tertiary interval, whereas magmatism occurred during Ectasian, Neoproterozoic,  
106 Cambrian–Ordovician, and Triassic–Tertiary intervals (Bookstrom et al., 2016 and references therein).

107         Co-Cu-Au occurrences of the ICB are hosted by the coarse siltite and banded siltite units of the  
108 Apple Creek Formation and the Gunsight Formation of the Lemhi Group (Fig. 1B; Fig. 2). In the ICB, the

109 coarse siltite unit consists mostly of biotitic siltite whereas the banded siltite unit comprises mostly  
110 interlayered siltite and biotite phyllite to schist (after argillite; Bookstrom et al., 2016). Depositional ages  
111 of these rocks are bracketed by the youngest sets of detrital zircons in samples from the underlying  
112 Hoodoo Formation (ca. 1445 Ma; Link et al., 2007) and from the uppermost part of the banded siltite unit  
113 (ca. 1409 Ma; Aleinikoff et al., 2012).

114 The granite pluton of Big Deer Creek, which bounds the northeastern margin of the ICB, belongs  
115 to a bimodal suite of A-type megacrystic granite and meta-gabbroid intrusions that was dated at  $1377 \pm 4$   
116 Ma (Aleinikoff et al., 2012). Gabbroid to syenitoid plutons (dated at 485–530 Ma; Lund et al., 2011;  
117 Gillerman, 2008) and chemically similar mafic dikes represent within-plate magmatism, inboard from the  
118 rifted continental margin, associated with early subsidence and growth of the Cordilleran miogeocline in  
119 Cambrian–Ordovician time (Evans, 1984; Lund et al., 2010; Bookstrom et al., 2016).

120 Structurally, the metasedimentary host rocks to the ICB, the granite pluton of Big Deer Creek, and  
121 the syenitoid Deep Creek plutons are within the Poison Creek thrust plate which is bounded by the Poison  
122 Creek and Iron Lake thrust faults of Cretaceous age (Fig. 1B, Fig. 3). Similarly, the Blackbird Co-Cu-Au  
123 deposit lies within a structural block between the Little Deer and White Ledge faults of Cretaceous age  
124 (Fig. 1B). Nold (1990) recognized that ore minerals and metasedimentary host rocks of the ICB are  
125 increasingly deformed, metamorphosed, and recrystallized from southeast to northwest (and from the fold-  
126 thrust belt to the hinterland of the East Kootenay orogen, as shown in Fig. 1A). Phyllitic biotite-chlorite-  
127 bearing rocks of greenschist facies at the southeast end of the ICB pass northwestward to schistose garnet-  
128 biotite-bearing rocks of lower-amphibolite facies in the northwest part of the Blackbird mine area, and to  
129 gneissic sillimanite-garnet-biotite-quartz rocks of upper-amphibolite facies at the northwest end of the  
130 ICB (Bookstrom et al., 2016). Inasmuch as the lower boundary of the garnet zone is gradational, it appears  
131 that the thermal gradient increases upward, possibly in the footwall of a hotter thrust plate that overrode  
132 the northwestern part of the ICB before being removed during uplift and erosion (Fig. 3). As a result of  
133 this tectono-thermal setting, three metamorphic and/or structural domains in this order upwards are  
134 sandwiched between the Poison Creek and Indian Creek faults: (1) the lowermost domain called the

135 “Haynes-Stellite domain” features lower to middle greenschist facies rocks, (2) then the “Blackbird  
136 domain” is characterized by middle to upper greenschist facies rocks and contains the Idaho and Chicago  
137 zones within the Blackbird mine, (3) and finally, the Indian Creek metamorphic domain characterized by  
138 upper greenschist to lower amphibolites rocks, and rocks above garnet isograd (Fig. 3; cf. Lund et al.,  
139 2011).

140

### 141 **3. Mineralization, available geochronological constraints and sampling**

#### 142 *Blackbird mine area*

143 The Blackbird mine is central to the ICB and contains at least 8 strata-bound and semi-concordant  
144 ore zones (e.g., Chicago and Idaho zones), several strata-bound prospects (e.g., Merle), and many  
145 prospects comprising discordant veins (e.g., Sunshine), mineralized breccias, and small replacement-style  
146 occurrences. A minimum estimate of total resources of the Blackbird district was reported by Slack (2013)  
147 as 16.8 Mt of ore, averaging 0.73% Co, 1.37% Cu, and 1 ppm Au. This estimate does not include  
148 downward projections of ore zones that are open down-dip.

149 In the Blackbird mine area, stratabound cobaltite-biotite ore zones  $\pm$  tourmaline are preferentially  
150 hosted in biotite-rich layers in banded siltite, which is folded into large- and small-scale chevron-style  
151 folds that plunge moderately northward. The Idaho Zone is located in the tight hinge zone of a large-scale  
152 syncline whereas the Chicago Zone lies in a thickened limb. Unaltered banded siltite consists of  
153 interlayered siltite and argillite, but in cobaltite-biotite ore, argillite is “altered” to biotitite, containing  
154 >75% of greenish-black biotite that is unusually rich in ferrous iron and chlorine, and is interpreted as  
155 hydrothermal biotite (Bookstrom et al., 2016). Two samples for Re-Os analysis were taken from (1) the  
156 tabular and vein-like body of the Chicago zone (CH) where alternating bands of massive and coarse-  
157 grained and fine-grained cobaltite are surrounded by greenish-black biotite, and, (2) the quartz-  
158 tourmaline-cobaltite breccias in the Idaho zone (ID; Bookstrom et al., 2016; Fig. 1B, Fig. 4).

159 Oscillatory-zoned xenotime grains intergrown with biotite in cobaltite-biotite ore, which formed  
160 at  $1370 \pm 4$  Ma as a late stage of hydrothermal activity related to intrusion of the Big Deer Creek granite,  
161 are found as inclusions in cobaltite at the Merle prospect (in situ U-Pb SHRIMP ages, Aleinikoff et al.,  
162 2012). These authors proposed that the first generation of cobaltite is thus younger than ca. 1370 Ma.  
163 Slack (2012) proposed that the 1370 Ma-old hydrothermal system responsible for xenotime growth may  
164 have also triggered precipitation of cobaltite (with xenotime inclusions), chalcopyrite and gold at a later  
165 stage. Additional Proterozoic xenotime precipitation occurred at 1315 to 1270 Ma and ca. 1050 Ma.  
166 However, no introduction of metals is reported during these time intervals in the Belt-Purcell basin  
167 (Aleinikoff et al., 2012).

168 Mafic dikes of probable Cambrian–Ordovician age cut older cobaltite-biotite lodes but are in turn  
169 cut by younger quartz-siderite-Fe-Cu-sulfide veins and breccias  $\pm$  minor cobaltian arsenopyrite. These Fe-  
170 Cu-sulfide-bearing veins and breccias are not folded and lack metamorphic fabrics (Bookstrom et al.,  
171 2016). Lund et al. (2011) determined a  $^{40}\text{Ar}/^{39}\text{Ar}$  age of  $83 \pm 1$  Ma for muscovite selvage around a pyrite-  
172 chalcopyrite-quartz vein at the Sunshine prospect. This Upper Cretaceous age is in accord with late Early  
173 Cretaceous ( $110 \pm 3$  Ma) to early Late Cretaceous ( $92 \pm 5$  Ma) in situ U-Pb SHRIMP ages of monazite  
174 enclosing cobaltite in places at the Merle prospect (Aleinikoff et al., 2012). This Cretaceous hydrothermal  
175 event also triggered the growth of xenotime grains or rims in conjunction with cobaltite. Garnets from the  
176 northwestern part of the ICB yield Lu-Hf late Upper Jurassic to Upper Cretaceous ages of ca. 151 to 94  
177 Ma (Zirakparvar et al., 2007). Garnet porphyroblasts in ore zones commonly contain cobaltite inclusions,  
178 which is consistent with a pre-Cretaceous age for cobaltite-biotite ore.

179

### 180 *Haynes-Stellite mine*

181 The Haynes-Stellite mine (HS in Fig. 1B) produced a small tonnage of cobaltite-rich ore from a pipe-like  
182 ore body in a NW-striking and steeply-dipping tabular quartz-tourmaline breccia, which cuts in quartzite  
183 with thin interbeds of biotite phyllite, near the base of the Gunsight Formation (which overlies the banded-  
184 siltite unit). The dated sample (Fig. 4) contains aligned lenticular clasts of quartz and quartz-tourmaline

185 breccia in a matrix of tourmaline with cobaltite stringers, interpreted to indicate streamlined flow foliation  
186 (Bookstrom et al., 2016).

187

### 188 *Black Pine mine and prospects*

189 The Black Pine mine and neighboring prospects are about 14 km southeast of the Blackbird mine (Fig.  
190 1B), where they are hosted in thin-bedded banded siltite, consisting of interlayered siltite and locally  
191 chloritized biotite phyllite (sample in Fig. 4). The lower level of the Black Pine mine followed thin  
192 concordant and discordant veins of the strata-bound copper zone, and the upper level followed the strata-  
193 bound cobalt zone. These mineralized zones and their host strata generally strike northwest and dip about  
194 60° northeast. Chalcopyrite, pyrite, and arsenopyrite are the main ore minerals, but quartz, siderite,  
195 cobaltian arsenopyrite, cobaltite, and magnetite siderite are also present in some veins and mineralized  
196 breccias (Nold, 1990; Bookstrom, 2013).

197

## 198 **4. Material and methods**

### 199 **4.1 Sample preparation**

200 A total of four samples of cobaltite mineralization from the Idaho Cobalt belt (Fig. 4) were  
201 processed prior to Re-Os isotope geochemistry: 1) tourmalinized breccia of quartz, biotite, K-feldspar,  
202 xenotime cemented by disseminated brownish pink cobaltite at the Haynes-Stellite deposit (HS, Fig. 4a);  
203 2) layers of massive coarse-grained to fine-grained brownish pink cobaltite ± xenotime at the Chicago  
204 Zone (CH, Fig. 4b), Blackbird mine; 3) layers of disseminated brownish pink cobaltite in a biotite, quartz,  
205 K-feldspar rock at the Idaho Zone (ID, Fig. 4c), Blackbird mine; and, 4) coarse-grained disseminated  
206 shiny grey cobaltite in a quartz-chlorite rock, Black Pine deposit (BP, Fig. 4d).

207 All samples were cut into slabs that were thoroughly cleaned using silicon carbide grit and paper to  
208 remove any metal traces left by hammering or sawing (Fig. 5). These samples were crushed using agate  
209 mortar and pestle and sieved through disposable home-made nylon sieves to produce 70–200 and +70

210 mesh size fractions. Following heavy liquid separation using Sodium Polytungstate (SPT, specific gravity  
211 of 2.86), a Frantz Isodynamic Separator was used to produce magnetic (M) and non-magnetic (NM)  
212 cobaltite fractions from the 70–200 mesh fractions by applying successive 0.3, 0.6 and 0.9 amp currents  
213 for all samples (except the Black Pine sample for which 1.8 and 2.1 amp currents had to be applied) with  
214 15° side slope and 10° forward slope. The composition of each mineral separate was verified by X-ray  
215 diffraction (XRD) analyses. Aliquots of each magnetic fraction were embedded in epoxy and the mounts  
216 were studied by scanning electron microscopy (SEM) using a Zeiss Sigma 300 Field Emission SEM (VP-  
217 FESEM) operated in backscattered electron mode (SEM-BSE, beam conditions of 15kV). In addition,  
218 a Bruker energy dispersive X-ray spectroscopy (EDS) system with dual silicon drift detectors each with an  
219 area of 60 mm<sup>2</sup> and a resolution of 123 eV was used for single spot analysis to further control the  
220 mineralogy of each mineral separate. After magnetic separation, the final mineral separates contained  
221 ~50–100% cobaltite, 0–50 % non-sulfide gangue minerals (e.g., xenotime, quartz, biotite) in all samples,  
222 and up to 1% native gold and <0.5% Bi-telluride in the case of the Chicago Zone sample.

223

## 224 **4.2 Cobaltite petrography and major and trace element chemistry of cobaltite**

225 Detailed petrography of each cobaltite fraction mounted in epoxy was complemented by major  
226 and trace element chemical analysis. Compositional analyses were performed on a Cameca SX-100  
227 electron microprobe equipped with 5 tunable wavelength dispersive spectrometers at the Department of  
228 Earth & Atmospheric Sciences, University of Alberta, Edmonton, Canada. Operating conditions were 40°  
229 take-off angle and a beam with energy of 20 keV, a current set at 20 nA, and a diameter of 2 microns.  
230 Elements were acquired using analyzing crystals LLIF for As K $\alpha$ , Co K $\alpha$ , Cu K $\alpha$ , Fe K $\alpha$ , Zn K $\alpha$ , Ni K $\alpha$ ,  
231 PET for Te L $\beta$ , Bi M $\alpha$ , Te L $\beta$  (2), Bi M $\alpha$  (2), S K $\alpha$ , and LTAP for Se L $\beta$ . The standards were Ni metal for  
232 Ni K $\alpha$ , Cu metal for Cu K $\alpha$ , Co metal for Co K $\alpha$ , gallium arsenide GaAs for As K $\alpha$ , bismuth telluride  
233 Bi<sub>2</sub>Te<sub>3</sub> for Bi M $\alpha$ , Te L $\beta$ , Bi M $\alpha$ , Te L $\beta$ , gallium selenide GaSe for Se L $\beta$ , iron disulfide FeS<sub>2</sub> for Fe K $\alpha$ ,  
234 and sphalerite ZnS for S K $\alpha$ , Zn K $\alpha$ . The counting time was 30 seconds for each element with an off peak  
235 counting time of 30 seconds. Off peak corrections were linear for all elements. Unknown and standard

236 intensities were corrected for deadtime whereas standard intensities were corrected for standard drift over  
237 time. Interference corrections were applied to S for interference by Co, and Te for interference by Cu (cf.  
238 Donovan et al., 1993). Detection limits (at the 99% confidence level) are 0.02 wt% for Co, Cu, S, and Zn,  
239 0.01 wt% for Fe, 0.03 wt% for Ni, 0.05 wt% for As, 0.07 wt% for Te, 0.09 wt% for Bi and 0.12 wt% for  
240 Se. The matrix correction method was ZAF or Phi-Rho-Z Calculations and the mass absorption  
241 coefficients dataset was LINEMU. The ZAF or Phi-Rho-Z algorithm utilized was Conventional  
242 Philibert/Duncumb-Reed (cf. Armstrong, 1988).

243

### 244 **4.3 Re-Os analytical procedure**

245 For each analysis, between 50 and 350 mg of cobaltite mineral separates was weighed and  
246 transferred into a thick-walled borosilicate Carius tube. Each sample was dissolved in inverse aqua regia  
247 (~2mL of 10 N HCl and ~6 mL 16 N HNO<sub>3</sub>) with a known amount of <sup>185</sup>Re+<sup>190</sup>Os spike solution at 210°C  
248 for 24 hours (Fig. 5). The full Re-Os laboratory protocol used in the present work is described in full in  
249 Hnatyshin et al. (2016). Re and Os isotopic compositions were determined by negative thermal ionization  
250 mass spectrometry (NTIMS) using a ThermoScientific Triton mass spectrometer at the Canadian Centre  
251 for Isotopic Microanalysis, University of Alberta, Edmonton, Canada. Rhenium was measured as ReO<sub>4</sub><sup>-</sup> in  
252 static mode on Faraday collectors, whereas Os was measured as OsO<sub>3</sub><sup>-</sup> in peak-hopping mode on SEM  
253 with a constant flow of oxygen (Creaser et al., 1991; Völkening et al., 1991; Hnatyshin et al., 2016).  
254 Measurement quality was monitored by repeated measurements of in-house Re (<sup>185</sup>Re/<sup>187</sup>Re = 0.59774 ±  
255 0.00065, n = 23) and Os (“AB-2 standard”, <sup>187</sup>Os/<sup>188</sup>Os = 0.10682 ± 0.00009, n = 100) standard solutions.  
256 Total procedural blanks for each set of samples are reported in Table 1.

257 All Re-Os ages are reported as Model 1 or Model 3 isochrons through regression in <sup>187</sup>Os/<sup>188</sup>Os vs.  
258 <sup>187</sup>Re/<sup>188</sup>Os space of the Re-Os data which are reported at the 2σ level (95% level of confidence). The  
259 *Isoplot* v 4.15 program (Ludwig, 2011) was used for isochron regression by considering the <sup>187</sup>Re decay  
260 constant of 1.666e<sup>-11</sup> year<sup>-1</sup> (Smoliar et al., 1996).

261

## 262 **5. Results**

### 263 **5.1 Petrography of the cobaltite mineral fractions**

264 SEM-BSE images of the different cobaltite mineral fractions studied are shown in Fig. 6. Mineral  
265 separates (M0.6, M0.9 and NM0.9) from the Chicago Zone are characterized by densely packed cobaltite  
266 grains (up to 15  $\mu\text{m}$  in width) with about 10 to 20% gangue minerals (mainly biotite) in the M0.6 and  
267 M0.9 fractions (Figs. 6a and b). The NM0.9 fraction corresponds to 95 % cobaltite with up to 5% gold  
268 whereas Bi-tellurides make up to 1–2% of the M0.6 and M0.9 separates (Figs. 6a, b and c). The unique  
269 M0.9 mineral fraction from Haynes-Stellite corresponds to cobaltite (70–80%, between 10 and 50  $\mu\text{m}$  in  
270 width), biotite, K-feldspar, quartz and xenotime (Figs. 6d and e). Xenotime postdates precipitation of  
271 cobaltite. Cobaltite crystals have sharp edge when in contact with gangue minerals but xenotime with  
272 which it is in contact along irregular, dented edges. The M0.3 and M0.6 mineral fractions from the Idaho  
273 Zone comprise ca. 5 to 10 % euhedral to subhedral cobaltite (between 5 to 35  $\mu\text{m}$  in width) embedded in  
274 gangue minerals, being mainly quartz, sulfur-bearing Na-silicate (tentatively suggested to being scapolite  
275 with a  $-\text{SO}_4$  component) and up to 3 to 4 % xenotime (Figs. 6g and h).

276

### 277 **5.2 Major and trace element chemistry of cobaltite mineral fractions**

278 A total of 159 analyses were performed on the 70–200 mesh size mineral fractions of cobaltite from  
279 the Chicago and Idaho Zones, the Haynes-Stellite deposit and the Black Pine prospect (Electronic  
280 Supplementary Material 1). Besides the major elements (Co, As, and S), Fe and Ni were detected in all  
281 studied fractions whereas Zn was sporadically detected (values  $< 0.03$  wt%) and Cu was only detected in  
282 the fractions from the Haynes-Stellite deposit ( $< 0.55$  wt%, Table 2). Selenium was not detected at all.  
283 Tellurium values are below 0.10 wt% whereas Bi values reach 0.2 wt% at maximum. Based on the  
284 mineralogy of the cobaltite mineral fraction, it is suggested that these elements are contributed by micro-  
285 inclusions of Bi-telluride, particularly in the case of the Chicago Zone (Fig. 6). Modal mineral formulae

286 were calculated for each fraction. The various fractions of each mineral deposit have similar compositions  
287 despite variable magnetic susceptibilities (Table 3). When considering the relative positions of the mineral  
288 deposit in the NW–SE striking Idaho Cobalt Belt and the metamorphic grade of each mineral deposit  
289 (Figs. 1B and 3), one notices that cobaltite in the north-westernmost Chicago Zone (middle to upper  
290 greenschist facies) has the lowest Co and highest Ni contents ( $S_{0.97-0.98}Fe_{0.06-0.07}Co_{0.88-0.89}Ni_{0.04}As_{1.03}$ ; Fig.  
291 7). Cobalt and Ni contents in cobaltite in the Idaho Zone, located in the same metamorphic domain as the  
292 Chicago Zone, has slightly higher Co and lower Ni contents ( $S_{0.99}Fe_{0.05-0.06}Co_{0.92-0.93}Ni_{0.02}As_{1.01}$ ). Cobaltite  
293 in the lowermost Haynes-Stellite structural block with lower to middle greenschist facies grade, has  
294 mineral composition in the range of that found in the Idaho Zone ( $S_{0.98}Fe_{0.05}Co_{0.92}Ni_{0.02}As_{1.02}$ ). Cobalt  
295 EMP mapping reveals that cobaltite in the Haynes-Stellite mineral fraction is oscillatory zoned with  
296 respect to Co (Fig. 6f). Outside the Blackbird domain, towards the southwest, cobaltite at Black Pine is  
297 devoid of Ni and has the highest Co contents encountered in the current work  
298 ( $S_{0.98}Fe_{0.05-0.06}Co_{0.94-0.95}Ni_{0.00}As_{1.02}$ ).

299

### 300 **5.3 Re-Os results for cobaltite mineral fractions**

301 Results for 4 trial analyses of cobaltite mineral separates from Black Pine did not yield reliable Re-Os  
302 isotope data because of low Re concentrations (< 0.3 ppb; Table 3). By contrast, the results of 23 Re-Os  
303 isotope analyses of cobaltite mineral separates from the Chicago Zone (n = 7), Idaho Zone (n = 10) and  
304 Haynes-Stellite (n = 6) are presented in full in Table 3. Osmium concentrations range from 12 to 64 ppt  
305 whereas Re concentrations range from 0.4 to 3.4 ppb. Uncertainties ( $\pm 2\sigma$ ) are 0.89% or better for Re  
306 abundances whereas they amount to 9.7% or better for Os, except seven outliers with uncertainties above  
307 12%. These outliers are readily explained by higher percentages of Re and Os blanks, with values above  
308 2.8% and 0.75%, respectively. Ratios of  $^{187}Re/^{188}Os$  vary from 512 to 1818. Ratios of  $^{187}Os/^{188}Os$  range  
309 from 17.4 to 44.2. These ratios are highly radiogenic and the mineral fractions of these deposits qualify as  
310 Low-Level Highly Radiogenic (LLHR) samples (cf. Stein et al., 2000). There is no trend of magnetic  
311 fractions having more radiogenic  $^{187}Os/^{188}Os$  ratios than the respective non-magnetic fractions (e.g.,

312 NM0.9 vs. M0.6 & M0.9 for the Chicago Zone) or “less” magnetic fractions (e.g., M0.6 vs. M0.3 in the  
313 Idaho Zone).

314 Data points for the Chicago Zone scatter greatly, not defining any cluster nor linear trend in a  
315  $^{187}\text{Re}/^{188}\text{Os}$  vs.  $^{187}\text{Os}/^{188}\text{Os}$  plot (Fig. 8). By contrast, data points for the Idaho Zone and the Haynes-  
316 Stellite deposit plot in particular fields of this diagram. Most data points for the Idaho Zone plot along or  
317 close to a 1100 Ma reference isochron (initial  $^{187}\text{Os}/^{188}\text{Os}$  ratio of 9) with two outliers closer to the 1200  
318 Ma reference isochron (same initial  $^{187}\text{Os}/^{188}\text{Os}$  ratio). By contrast, data points for the Haynes-Stellite  
319 deposit plot close to a 1300 Ma reference isochron (initial  $^{187}\text{Os}/^{188}\text{Os}$  ratio of 5) with two outliers plotting  
320 close to a 1500 Ma reference isochron (same initial  $^{187}\text{Os}/^{188}\text{Os}$  ratio). The ten data points for the Idaho  
321 Zone define a Model 3 isochron with an age of  $1105 \pm 240$  Ma ( $2\sigma$ ; mean squared weighted deviates,  
322  $\text{MSWD} = 7.5$ , initial  $^{187}\text{Os}/^{188}\text{Os}$  ratio  $[\text{Os}]_i = 9.5 \pm 2.9$ ; Fig. 9). However, three data points display  
323 extremely large error ellipses. These uncertainties are explained by high Re blank contribution for these  
324 analyses (Table 3). Regression of the seven other data points yields a Model 3 isochron with an age of  
325  $1132 \pm 240$  Ma ( $2\sigma$ ;  $\text{MSWD} = 9.3$ , initial  $^{187}\text{Os}/^{188}\text{Os}$  ratio  $[\text{Os}]_i = 9.0 \pm 2.9$ ). The four data points of  
326 Haynes-Stellite cobaltite that plot close to the 1300 Ma reference isochron all have aliquot weights above  
327 200 mg. These data points define a Model 1 isochron with an age of  $1349 \pm 76$  Ma ( $2\sigma$ ;  $\text{MSWD} = 2.1$ ,  
328 initial  $^{187}\text{Os}/^{188}\text{Os}$  ratio  $[\text{Os}]_i = 4.7 \pm 2.2$ ; Fig. 10). The two outliers mentioned above have aliquot weights  
329 of 50 and 145 mg and present large uncertainties and extended error ellipses due to high Re blank  
330 contribution (even high Os contribution in the case of the aliquot with weight of 50 mg; Table 3).

331

## 332 **6. Discussion**

### 333 **6.1 Cobaltite petrography, chemistry, metamorphism and validation of Re-Os isochron** 334 **ages**

335 In the Chicago Zone, the alternating bands of close-packed fine-grained and coarse-grained massive  
336 cobaltite (Figs. 4b, 6) were interpreted as a product of recrystallization of pre-existing cobaltite

337 mineralization in response to Cretaceous metamorphism (Bookstrom et al., 2016), producing cross-aligned  
338 cobaltite fabrics shown in Fig. 4b. Our results support this interpretation. This cobaltite metamorphosed to  
339 middle to upper greenschist facies has the lowest Co and the highest Ni content of the study (Fig. 3, Table  
340 2). We suggest that Co was lost from cobaltite and retained in the rock in other minerals during prograde  
341 metamorphism. This mechanism would explain the relative Co-enrichment of biotite hornfels in the  
342 Blackbird area (i.e., 19 ppm Co; Connor, 1991; Bookstrom et al., 2016), thereby implying that these rocks  
343 are not the source of metals but became rather enriched in metals as a result of metal redistribution during  
344 metamorphism. This preferred interpretation is supported by a similar pattern observed in pyrite and other  
345 sulfide minerals in unmetamorphosed to amphibolites facies-metamorphosed greywackes in the Otago and  
346 Alpine Schists of New Zealand (Pitcairn et al., 2010). These authors observed that prograde  
347 metamorphism and breakdown of pyrite to pyrrhotite was accompanied by a redistribution of Co and Ni  
348 that remained in the rock and were incorporated in other sulfide minerals than pyrite. Whereas Co was  
349 probably lost to biotite hornfels during prograde metamorphism in the Blackbird area, Ni was enriched in  
350 cobaltite in the Chicago Zone. Although it would be tempting to link this Ni-enrichment to the presence of  
351 pyrrhotite that was observed in other samples of the Chicago Zone (cf. Bookstrom et al., 2016), no  
352 pyrrhotite inclusions were observed in cobaltite in the studied sample. The significant scatter of the Re-Os  
353 data for the Chicago Zone in the  $^{187}\text{Re}/^{188}\text{Os}$ - $^{187}\text{Os}/^{188}\text{Os}$  space would logically be expected for cobaltite  
354 that recrystallized during metamorphism and underwent disturbance of the Re-Os chronometer.  
355 Disturbance of the chronometer during metamorphism would be expected to result in mixed signatures of  
356 the metamorphic fluid and the primary Re-Os budget in cobaltite. A diagram of  $^{187}\text{Os}/^{188}\text{Os}$  vs.  $1/^{192}\text{Os}$   
357 using “common”  $^{192}\text{Os}$  rather than total Os (including radiogenic ingrowth of  $^{187}\text{Os}$ ) enables a fair  
358 assessment of mixing (van Acken et al., 2014). Some degree of mixing may be observed in the pseudo-  
359 linear trend of the Chicago Zone data points in such a diagram (labeled “CH-x” in Fig. 11, green ellipse).  
360 The absence of isochronous behavior of the data and evidence of mixing with metamorphic fluid suggest  
361 significant disturbance of the system that cannot even be exploited to determine the timing of this  
362 disturbance (Figs. 8 and 11).

363 Fine-grained cobaltite from the Haynes-Stellite deposit is oscillatory-zoned with respect to Co with  
364 Co contents varying over 5wt. % (Table 2, Figs. 6f and 7). Within the lower to middle greenschist  
365 Haynes-Stellite structural block (Fig. 3), cobaltite shows limited recrystallization as illustrated by  
366 coexisting very fine-grained grains (<10  $\mu\text{m}$ ) in between a few larger cobaltite crystals (ca. 20 to 50  $\mu\text{m}$ ;  
367 Fig. 6). An isochronous behavior is only observed for 4 Re-Os data points of fine-grained cobaltite that  
368 correspond to aliquots with weight above 200 mg (Fig. 8). The other two data points corresponding to  
369 aliquots of ca. 50 and 150 mg deviate towards older ages in the range of 1500 Ma (Fig. 8, Table 3). We  
370 suggest that sampling cobaltite from Haynes-Stellite to a minimum aliquot size of 200 mg overcomes the  
371 possible, yet minor, disturbance of the Re-Os budget in cobaltite by this limited recrystallization during  
372 lower to middle greenschist metamorphism. Indeed, the isochronous behavior of the 4 data points for  
373 aliquots of at least 200 mg combined with the absence of linear correlation in  $^{187}\text{Os}/^{188}\text{Os}$ -1/ $^{192}\text{Os}$  space  
374 (Figs. 8 and 11) indicate that Re-Os systematics were preserved in cobaltite at Haynes-Stellite, and, the  
375 late Mesoproterozoic (ca. 1349 Ma) age may be further interpreted in the next section.

376 To end with, fine-grained cobaltite from the Idaho Zone has an extremely uniform chemical  
377 composition whatever the mineral fraction (i.e., M 0.3 and M 0.6; Fig. 7 and Table 2). In both fractions, in  
378 particular the M 0.6 fraction, cobaltite shows evidence of recrystallization of formerly very fine-grained  
379 cobaltite grains (<10  $\mu\text{m}$ ) that coalesced together to produce coarser-grained cobaltite (ca. 20  $\mu\text{m}$ )  
380 embedded in silicates  $\pm$  xenotime (Fig. 6h). Given the position of the Idaho Zone within the same middle  
381 to upper greenschist metamorphic facies structural block as the Chicago Zone (Fig. 3), it is likely that the  
382 Re-Os budget of cobaltite was either reset or completely disturbed without any age information. Yet, the  
383 isochronous behaviour of the seven data points of the Idaho Zone with low-uncertainty ellipses and the  
384 lack of linear correlation in the  $^{187}\text{Os}/^{188}\text{Os}$ -1/ $^{192}\text{Os}$  space (Figs. 7 and 11) imply that the  $1132 \pm 240$  Ma  
385 age is meaningful and is interpreted geologically in the next section.

386  
387 **6.2 From Middle Mesoproterozoic cobaltite mineralization to Grenvillian and Cordilleran**  
388 **metamorphic overprint**

389 A summary of events from the formation of the Belt Basin in Early Mesoproterozoic to the  
390 compressive tectonics of the Cordilleran fold-and-thrust belt is proposed in Fig. 12. Although the cobaltite  
391 Re-Os age of  $1349 \pm 76$  Ma for the Haynes-Stellite deposit is associated with a relatively large uncertainty  
392 ( $\sim \pm 5.6\%$ ,  $2\sigma$ ), due primarily to the limited range of  $^{187}\text{Re}/^{188}\text{Os}$  and  $^{187}\text{Os}/^{188}\text{Os}$  ratios (Fig. 8, Table 3), it  
393 is consistent with existing constraints for a middle Mesoproterozoic sulfide mineralization in the Idaho  
394 Cobalt Belt. Overall, this age agrees with a tectonic and plutonic engine for mineralization related to the  
395 East Kootenay orogeny (ca. 1379 to 1325 Ma). Our Re-Os age is younger than the youngest SHRIMP U-  
396 Pb detrital zircon age ( $1409 \pm 10$  Ma) constraining the maximum age of the host sedimentary unit at  
397 Haynes-Stellite (Gunsight Formation, Fig. 2; Aleinikoff et al., 2012; Bookstrom et al., 2016). In addition,  
398 this age draws a connection with the emplacement of bimodal gabbro-granite suite of plutons between ca.  
399 1383 and 1359 Ma (Anderson and Davis, 1995; Evans et al., 2000; Aleinkoff et al., 2012). In particular, a  
400 timing for cobaltite mineralization at ca. 1349 Ma supports the proposal of Slack (2012) that sulfide  
401 mineralization may have occurred in connection with the emplacement of the Big Deer Creek granite  
402 dated at  $1377 \pm 4$  Ma (Aleinikoff et al., 2012). This granite is presently found in the Haynes-Stellite  
403 structural block (Fig. 3) and originally intruded into the host rocks to the Haynes-Stellite deposit.  
404 Aleinikoff et al. (2012) and Slack (2012) convincingly connected the precipitation of xenotime in the  
405 Apple Creek Formation with the emplacement of the Bid Deer Creek granite. Of particular interest is the  
406 oldest generation of xenotime dated at  $1370 \pm 4$  Ma that locally forms inclusions in cobaltite (e.g., Merle  
407 deposit, Fig. 3; Aleinikoff et al., 2012), suggesting that cobaltite is younger than ca. 1370 Ma at the Merle  
408 deposit. Our ca. 1349 Ma Re-Os age, although not produced from cobaltite with xenotime inclusions dated  
409 at ca. 1370 Ma as at Merle, indicates timing of Co-sulfide mineralization shortly after a phase of REE-Y  
410 mineralization in connection with the emplacement of the Big Deer Creek granite at ca. 1370 Ma, as  
411 originally proposed by Slack (2012) in his effort to explain the close textural association of cobaltite and  
412 xenotime in many samples from the district. It is also agrees with the bracketing of formation of the  
413 quartz-tourmaline-cobaltite breccia between 1370 and 1320 Ma proposed by Bookstrom et al. (2016) in  
414 their synthesis of the geologic history of the Blackbird mine area based on observed relative age

415 relationships and available isotope age determinations on gangue minerals. In the light of this independent  
416 data and our Re-Os age of ca. 1349 Ma, we propose that the Haynes-Stellite cobaltite mineralization was  
417 formed in middle Mesoproterozoic time. The Re-Os isotopic system closed in this mineral at that time  
418 without being disturbed or reset by Grenvillian metamorphism (ca. 1190 to 1006 Ma) nor by tectonism,  
419 metamorphism, and plutonism associated with Cordilleran orogenesis in Early to Late Cretaceous time  
420 (ca. 151 Ma to 83 Ma; Bookstrom et al., 2016 and references therein) in this sample.

421         The imprecise age for mineralization in the Idaho Zone ( $1132 \pm 240$  Ma, 21%,  $2\sigma$ ) overlaps within  
422 uncertainty with the age of cobaltite mineralization at Haynes-Stellite. However, three arguments favor the  
423 interpretation that this age records a younger event for the Idaho Zone that is distinct from that of the  
424 Haynes-Stellite deposit: (1) cobaltite in the Idaho Zone has at least 3 times less Re than cobaltite at  
425 Haynes-Stellite (Table 3), (2) the data points for each of these deposits define separate clusters in the  
426  $^{187}\text{Re}/^{188}\text{Os}$ - $^{187}\text{Os}/^{188}\text{Os}$  space (Fig. 8), and, (3) the initial  $^{187}\text{Os}/^{188}\text{Os}$  ratios for cobaltite in these deposits  
427 are distinct within error (Figs. 9 and 10). In addition, the strongest evidence for a younger event in the  
428 Idaho Zone than at Haynes-Stellite is that of Bookstrom et al. (2016) who proposed that unlike the quartz-  
429 tourmaline-cobaltite breccia at Haynes-Stellite, the quartz-tourmaline-breccia of the Idaho Zone parallels  
430 axial planar  $S_2$  cleavage of  $F_2$  folds, and, is coeval with a phase of cobaltite-xenotime precipitation  
431 bracketed at 1058 to 990 Ma. Our Re-Os age, albeit imprecise, overlaps with the timing proposed by  
432 Bookstrom et al. (2016) and corresponds to the time span of the Grenvillian orogeny. Although the  
433 Grenvillian orogen in present-day Sweden and eastern Canada is not known to be productive in terms of  
434 mineral deposits (Stephens M.B., pers. comm., 2015), evidence for regional Grenville-age metamorphism  
435 in western Laurentia continues to accumulate (cf. Zirkparvar et al., 2010; Vervoort et al., 2015).  
436 Arsenopyrite from the main ore stage silver mineralization in the Galena Mine in the neighboring Coeur  
437 d'Alene district, Idaho yielded a Re-Os age of ca. 1220 Ma, i.e., a Grenvillian age (Arkadaskiy et al.,  
438 2009). Other evidence of hydrothermal mineral precipitation of Grenvillian age was brought by Aleinikoff  
439 et al. (2015) with xenotime precipitation at sub-greenschist temperatures in the upper section of the Belt  
440 Supergroup at about 1160-1050 Ma. Given the relationship between the quartz-tourmaline-breccia in the

441 Idaho Zone and axial planar cleavage and fold, our tentative interpretation would suggest that a proto-ore  
442 which formed in the middle Mesoproterozoic (as in the case of the Haynes-Stellite quartz-tourmaline-  
443 cobaltite breccias) was affected by dynamothermal events (above 400°C as implied by the presence of  
444 garnet) during the Grenvillian orogeny. The Re-Os isotopic system in cobaltite in the Idaho Zone was  
445 reset above 400°C to yield a Grenvillian, yet, highly imprecise age. The uncertainty is primarily due to the  
446 relatively low Re and radiogenic  $^{187}\text{Os}$  contents. If the Idaho Zone originally formed at the same time as  
447 Haynes-Stellite, then Re (and Os) would have been lost during Grenvillian resetting thereby explaining the  
448 current Re and Os contents in cobaltite in the Idaho Zone with a much younger late Mesoproterozoic age.  
449 To end with, the Grenvillian age recorded by the Re-Os isotopic system in the Idaho Zone was preserved  
450 despite incorporation of this deposit in the Blackbird domain (Fig. 3) where metamorphic grade reached  
451 middle to upper greenschist facies in Cretaceous time.

452 The Chicago Zone failed to be dated by the isochron method and mixing between the Re-Os budget  
453 of cobaltite and later hydrothermal fluid is suggested. Yet, the highly radiogenic  $^{187}\text{Re}/^{188}\text{Os}$  and  
454  $^{187}\text{Os}/^{188}\text{Os}$  ratios in the range of those encountered at Haynes-Stellite and in the Idaho Zone favor a  
455 middle Mesoproterozoic proto-ore in which the Re-Os isotopic system was severely disturbed post-  
456 mineralization. Given the evidence of recrystallization of most cobaltite during Cretaceous metamorphism  
457 (Aleinikoff et al., 2012 in Slack, 2012), it is likely that the scatter in the Re-Os data (Fig. 8) observed in  
458 recrystallized fine- to coarse-grained cobaltite (Fig. 4 and Fig. 6) is the result of Cretaceous  
459 dynamothermal events and compressive tectonics (i.e., shear zone hosting the Chicago Zone). According  
460 to Eiseman (1988), Cretaceous metamorphism reached 400 to 520°C. Given the disturbance of the Re-Os  
461 isotopic system in cobaltite in the Chicago Zone, this temperature range is therefore concluded as being  
462 above the closing temperature for Re-Os in cobaltite.

463 The origin of coarse-grained cobaltite associated with cobaltian arsenopyrite in chloritized biotite  
464 phyllite remains unknown. A highly tentative hypothesis would consider that the small high-grade Black  
465 Pine deposit (1.0 Mt at 4.5 wt%, 0.08 wt% Co, and 1.03 g/t Au; Johnson et al., 1998) is a by-product of  
466 metamorphism and re-deposition of metals originally contained in Mesoproterozoic cobaltite ores of the

467 Blackbird area. Indeed, the mineral chemistry of cobaltite at Black Pine is the richest in cobalt in the  
468 current study and is devoid of Ni. Considering our interpretation for the Chicago Zone that cobalt was  
469 released during metamorphism while Ni was proportionally enriched, cobalt would have been re-deposited  
470 elsewhere, i.e., possibly towards the distal Black Pine site, where temperature and pressure levels were  
471 lower as indicated by lower metamorphic grade. In addition to enriching biotite hornfels in cobalt, it is  
472 possible that (Cretaceous?) metamorphism caused the formation of small high-grade deposit in NW-  
473 striking northwest and steeply NE-dipping strata like Black Pine.

474

### 475 **6.3 Preferred genetic model for Mesoproterozoic cobaltite mineralization in the light of** 476 **the new Re-Os isotope geochemistry data**

477 Considering the new Re-Os ages which indicate primary cobaltite mineralization in middle  
478 Mesoproterozoic during the East Kootenay orogeny with reworking during the Grenvillian orogeny and/or  
479 the Cordilleran orogeny (Fig. 12), we propose to refine the genetic model for cobaltite mineralization in  
480 the Idaho Cobalt Belt. By contrast to a trend in modern geology with an urge to classify ore deposits in  
481 “boxes” with acronyms that get often misused, we choose to adopt a purely descriptive approach by  
482 synthesizing existing literature data and new Re-Os data within the geologic framework of the engine that  
483 was the East Kootenay orogeny, followed by regional metamorphism in Grenvillian time, and by  
484 Cordilleran metamorphism, deformation, and plutonism in Late Jurassic to Late Cretaceous time. Any  
485 attempt to classify these deposits according to deposit-types (e.g., IOCG, Iron Oxide Copper-Gold) should  
486 “see through” metamorphism, and, take into account the established reaction of sulfide (e.g., pyrite)  
487 destabilization and H<sub>2</sub>S devolatilization during prograde metamorphism, i.e., pyrite → pyrrhotite + H<sub>2</sub>S →  
488 magnetite + H<sub>2</sub>S.

489 As originally proposed by Slack (2012), cobaltite mineralization in the Idaho Cobalt Belt is indeed  
490 an expression of multistage hydrothermal mineralization related to a magmato-hydrothermal system.  
491 Although the middle Mesoproterozoic ca. 1349 Ma age for cobaltite mineralization applies to the Haynes-  
492 Stellite tourmalinized breccias, mineralogical and geochemical ties between mineralization of these

493 breccias and the strata-bound sulfide deposits of the Blackbird district have been put forward by Slack  
494 (2012) and include: (1) the presence of abundant xenotime with cobaltite locally in both deposit types  
495 (Slack, 2012; our Fig. 6), (2) additional links in the similarity of boron isotope values ( $\delta^{11}\text{B} = -6.9$  to  
496  $+3.2\%$ ) determined for the breccia-hosted tourmalines and those within the strata-bound sulfide deposits  
497 such as within the Idaho Zone (Trumbull et al., 2011; Slack, 2012). Hence, we propose that Co-Cu-Au  
498 sulfide deposits were produced as part of an epigenetic Co-Cu-Au-Bi-Y-REE mineralizing system in  
499 connection with the emplacement of a ca. 1383 to 1359 Ma suite of bimodal gabbro-granite intrusions, in  
500 particular the Big Deer Creek granite dated at  $1377 \pm 4$  Ma (Slack, 2012; Aleinikoff et al., 2012). The  
501 mineralizing system would have deposited first Y, REEs and Be-bearing minerals (xenotime, gadolinite-  
502 (Y)) within these deposits at  $1370 \pm 4$  Ma (Slack, 2012; Aleinikoff et al., 2012). The second phase of  
503 mineralization consisted in the precipitation of cobaltite, and possibly, by extension, deposition of the Cu-  
504 sulfides. Given the fact that cobaltite mineralization occurred prior to Cretaceous metamorphism, a valid  
505 genetic model must see through the present metamorphosed rocks and metamorphic minerals to  
506 understand what were the conditions at the time of mineralization by documenting the origin and  
507 composition of the three key ingredients for mineralization: (1) hydrothermal fluids, (2) source of sulfur,  
508 and (3) source of metals.

509 Landis and Hofstra (2012) proposed that the hydrothermal fluid trapped in gangue quartz associated  
510 with cobaltite mineralization was a mixture of evaporated seawater and subordinate magmatic fluid.  
511 Trumbull et al. (2011) proposed that hydrothermal fluids at a formational temperature of  $300^\circ\text{C}$  and an  
512 boron isotopic of  $-7$  to  $3\%$  originated from marine carbonates and/or evaporitic marine borates;  
513 chemogenic sediments that are currently found in form of scapolite-tourmaline beds in the Yellowjacket  
514 and Apple Creek Formations (Fig. 1A; Tysdal and Desborough, 1997; Tysdal et al., 2003). The presence  
515 of evaporitic marine borates is compatible with the equatorial paleolatitudes that existed in the  
516 Mesoproterozoic (Landis and Hofstra, 2012). We suggest that intrusion of the Big Deer Creek granite at  
517 ca. 1377 Ma put these evaporitic fluids in motion and these mixed with magmatic-related fluids as

518 indicated by mantle-derived  $^3\text{He}$  and fluorine-derived  $^{22}\text{Ne}$  compositions of volatiles trapped in the same  
519 gangue quartz (Landis and Hofstra, 2012).

520 The initial  $^{187}\text{Os}/^{188}\text{Os}$  ratio determined through isochron regression reflects the origin of bulk Os  
521 incorporated in a mineral at the time of precipitation prior to ingrowth of radiogenic  $^{187}\text{Os}$  below the  
522 blocking temperature of the Re-Os system in the given mineral (e.g., Walker et al., 1991). By extension, it  
523 may be used to trace the source of metals and cobalt in the present case study. The extremely high initial  
524  $^{187}\text{Os}/^{188}\text{Os}$  ratio for the Haynes-Stellite deposit ( $4.7 \pm 2.2$ ) points to Archean and Paleoproterozoic source  
525 rocks from which Os (and metals) would have been derived. The Idaho Cobalt Belt in the Lehmi sub-  
526 basin is underlain by a NE–SW striking corridor of Laurentian basement rocks of the Great Falls tectonic  
527 zone which is sandwiched between the 3.2–2.8 Ga Medicine Hat block in the north and the >2.5 Ga  
528 Wyoming Craton in the south (Fig. 1B; Vervoort et al., 2015; Wang, 2015; Kilian et al., 2016). The Great  
529 Falls tectonic zone comprises Paleoproterozoic oceanic island-arc terrane which is in turn underlain by a  
530 very thick mafic body interpreted from seismic data (Foster et al., 2006). These Paleoproterozoic  $\pm$   
531 Archean rocks with overall mafic affinity appear as sound candidates able to supply metals like Co for  
532 mineralization. Arsenopyrite in the Galena mine has similarly high initial  $^{187}\text{Os}/^{188}\text{Os}$  ratio of ca. 6.  
533 Although arsenopyrite accompanying silver mineralization in the Galena mine is younger (ca. 1220 Ma;  
534 Arkadaskiy et al., 2009) than cobaltite mineralization at Haynes-Stellite, the similar range of initial ratio  
535 suggest derivation of metals from also these Paleoproterozoic to Archean rocks for mineralization in the  
536 Coeur d'Alene district, or else possibly, from older (ca. 1400 to 1500 Ma) ore deposits equivalent of the  
537 Sullivan deposit of British Columbia (Fleck et al., 2002) in which metals might have previously been  
538 mobilized from these Paleoproterozoic to Archean rocks.

539 Our interpretation is compatible with the uniform sulfur isotope values of cobaltite throughout the  
540 Blackbird district ( $8.0 \pm 0.4\text{‰}$ ) that was interpreted as sulfur being sourced from deep, crustal, highly  
541 metamorphosed  $\pm$  magmatic rocks (Johnson et al., 2012). Sulfur isotopic homogenization would have  
542 occurred during transport of possibly aqueous  $\text{H}_2\text{S}$  in the mixed hydrothermal fluids described above  
543 (Johnson et al., 2012; this study). Thus, considering that this mixture of magmatic and evaporated-

544 seawater-derived hydrothermal fluids transported both metals and reduced sulfur, the only viable  
545 precipitation mechanism for sulfide mineralization is cooling, as originally proposed by Johnson et al.  
546 (2012). The biotite zones (up to 1.87 wt% Cl in biotite) spatially and paragenetically associated with  
547 sulfide mineralization would thus represent metamorphosed alteration zones in which Fe- and Cl-rich  
548 hydrothermal fluids reacted with aluminous clastic sediments to form abundant Cl-rich Fe biotite (Slack,  
549 2012). Both hydrothermal alteration envelopes and sulfides were deformed during Cretaceous deformation  
550 that produced biotites.

551         Following primary cobaltite mineralization in middle Mesoproterozoic at ca. 1349 Ma, cobaltite  
552 mineralization was locally remobilized along  $S_2$  cleavages during the Grenvillian orogeny at ca.  $1132 \pm$   
553 240 Ma, as in the case of the quartz-tourmaline-cobaltite breccia in the Idaho Zone (Fig. 12).  
554 Remobilization of pre-existing middle Mesoproterozoic cobaltite mineralization with high initial  
555  $^{187}\text{Os}/^{188}\text{Os}$  ratio of ca. 5 is a preferred interpretation in order to explain cobaltite mineralization in the  
556 Idaho Zone with an initial ratio at ca. 9 and much lower Re contents than in older cobaltite at Haynes-  
557 Stellite (Fig. 9).

558         The final stage of cobaltite mineralization consists of a Cretaceous overprint (Fig. 12), recorded in  
559 the massive cobaltite from the Chicago Zone. Although most cobaltite in the Blackbird district was  
560 affected by lower to upper greenschist metamorphism, recrystallization and local remobilization  
561 (Bookstrom et al., 2007), Re-Os isotope systematics were preserved in those cobaltite deposits that were  
562 not affected by temperatures above 400°C. Cretaceous overprint would have reset the Pb isotopic  
563 composition of sulfides in the Blackbird district at ca. 100 Ma (data in Panneerselvam et al., 2012). The  
564 Pb isotopic composition of chalcopyrite at the Black Pine prospect (Panneerselvam et al., 2012) and our  
565 interpretation of the Re-Os budget and mineral chemistry in this small high-grade deposit favor the  
566 original idea of Bookstrom et al. (2007, 2016) that satellite deposits like Black Pine and Iron Creek (Fig.  
567 1A) represent Cretaceous remobilization in structures of pre-existing cobaltite mineralization. Most of  
568 these prospects, besides Black Pine where cobaltite is identified, do not contain cobaltite but cobaltian  
569 arsenopyrite and cobaltian pyrite in addition to pyrite and chalcopyrite. This interpretation is in line with

570 the presence of late quartz-pyrite-chalcopyrite veins in the Sunshine deposit with muscovite selvage that  
571 was dated as having formed at ca. 83 Ma.

572

## 573 **5 Conclusions**

574 In the present study, we have constrained for the first time the Re-Os systematics in cobaltite and  
575 produced Re-Os ages for cobaltite mineralization in two of the four studied deposits hosted by  
576 metasedimentary rocks of the Idaho Cobalt Belt (ICB), Idaho, USA (i.e., Haynes-Stellite deposit, Chicago  
577 and Idaho Zones of the Blackbird mine, Black Pine prospect). The results of our work are fourfold:

- 578 1. Variably magnetic fractions of cobaltite in the ICB have low Re and total Os contents (ca. 0.4–4  
579 ppb and 14–64 ppt, respectively) but elevated  $^{187}\text{Re}/^{188}\text{Os}$  (600–1800) and highly radiogenic  
580  $^{187}\text{Os}/^{188}\text{Os}$  (17–45) ratios. The Black Pine prospect has too low Re concentrations (<0.3 ppb) to  
581 produce any reliable Re-Os data. By contrast, Re-Os data of cobaltite from the quartz-tourmaline-  
582 cobaltite breccia Haynes-Stellite deposit are accurate and reproducible providing a minimum  
583 aliquot size of 200 mg whereas data for cobaltite from the quartz-tourmaline-cobaltite breccia of  
584 the Idaho Zone require a minimum aliquot size of 150 mg.
- 585 2. The Re-Os systematics in cobaltite at Haynes-Stellite and at the Idaho Zone are preserved and Re-  
586 Os data are regressed using the isochron approach. By contrast, the Re-Os systematics of cobaltite  
587 in the Chicago Zone are disturbed and a linear array of mixing with post-depositional  
588 hydrothermal fluids is identified in the  $^{187}\text{Os}/^{188}\text{Os}$  vs.  $1/^{192}\text{Os}$  space. Cobaltite was primarily  
589 deposited in the ICB at Haynes Stellite at  $1349 \pm 76$  Ma and was preceded by REE-Y-mineral  
590 precipitation at ca. 1370 Ma in connection with the emplacement of the Big Deer Creek granite at  
591 ca. 1377 Ma as part of a suite of bimodal magmatic activity between ca. 1383 and 1359 Ma  
592 (Aleinikoff et al., 2012). We propose that our age of  $1132 \pm 240$  Ma for cobaltite in the quartz-  
593 tourmaline breccia in the Idaho Zone and consideration of other geologic and structural

594 constraints (Bookstrom et al., 2007, 2016) illustrate a remobilization phase of pre-existing  
595 cobaltite mineralization along cleavages and folds during the 1190–1006 Ma Grenvillian orogeny.

596 3. Cobaltite formed at ca. 1349 Ma upon cooling at an inferred temperature of  $\leq 300^{\circ}\text{C}$  of a mixture  
597 of Mesoproterozoic evaporitic brines and magmatic fluids that carried both metals and reduced  
598 sulfur. The extremely high initial Os ratio derived from regression of the Re-Os data at Haynes-  
599 Stellite ( $4.7 \pm 2.2$ ) is used a tracing tool to identify the source of metals. The most likely scenario  
600 considers that metals were derived from lower crustal mafic source rocks of probable Archean  
601 age, overlain by oceanic island-arc rocks of Paleoproterozoic age, which are tectonically  
602 interlayered with Archean rocks of the Wyoming Province continental nucleus, in the collisional  
603 Great Falls tectonic zone, which projects beneath the Idaho Cobalt Belt. This scenario is  
604 compatible with the sulfur isotopic composition of cobaltite ( $+8.0 \pm 0.4\text{‰}$ ) that is best explained  
605 by reduced sulfur being sourced from deep, crustal and highly metamorphosed rocks (Johnson et  
606 al., 2012).

607 4. We propose that the Re-Os isotope system in cobaltite in the Chicago Zone, located in a middle  
608 greenschist facies metamorphic zone, may have been subjected to temperatures of 400 to 520°C  
609 proposed for Cretaceous garnet-bearing rocks of a lower amphibolites facies metamorphic domain  
610 above the domain hosting the Chicago Zone. A maximum closing temperature of 400°C is  
611 inferred for Re-Os in cobaltite. By contrast, cobaltite at Haynes-Stellite and the Idaho Zone, which  
612 underwent middle to lower greenschist Cretaceous metamorphism, preserved Mesoproterozoic  
613 age information delivered by the Re-Os isotope system.

614

## 615 **6 Acknowledgments**

616 This study was supported financially through a Swiss SNF Early Postdoc.Mobility Grant awarded to  
617 Nicolas J. Saintilan (NJS; P2GEP2\_162075), and, an NSERC Discovery Grant awarded to Robert A.  
618 Creaser (RAC). We thank George Lusher and Brett Riggan (Blackbird Mine Group) and Bill Scales and  
619 George King (Formation Metals Inc.) for permission to visit, study, and collect samples within the gated

620 Blackbird-mine. NJS and RAC thank the staff at USGS Office in Spokane for welcoming them during two  
621 short visits. NJS thanks Andrew Locock (University of Alberta) for his help and technical support for  
622 acquisition of microprobe data.

## 623 **7 References**

- 624 Aleinikoff, J.N., Slack, J.F., Lund, K., Evans, K.V., Fanning, C.M., Mazdab, F.K., Wooden, J.L., and Pillers, R.M.,  
625 2012. Constraints on the timing of Co-Cu+Au mineralization in the Blackbird district, Idaho, using SHRIMP U-  
626 Pb ages of monazite and xenotime plus zircon ages of related Mesoproterozoic orthogneisses and  
627 metasedimentary rocks. *Econ. Geol.* 107 1143-1175.
- 628 Aleinikoff, J.N., Lund, K., and Fanning, M.C., 2015. SHRIMP U-Pb and REE data pertaining to the origins of  
629 xenotime in Belt Supergroup rocks: evidence for ages of deposition, hydrothermal alteration, and  
630 metamorphism. *Can. J. Earth Sci.* 52, 722-745.
- 631 Anderson, A.L., 1947. Cobalt mineralization in the Blackbird district, Lemhi County, Idaho. *Econ. Geol.* 42, 22-46.
- 632 Anderson, H.E., and Davis, D.W., 1995. U-Pb geochronology of the Moyie sills, Purcell Supergroup, southeastern  
633 British Columbia: Implications for Mesoproterozoic geological history of the Purcell (Belt) Basin. *Can. J. Earth*  
634 *Sci.* 32, 1180-1193.
- 635 Arkadakskiy, S.V., Creaser, R.A., Richards, J.P., Hnatyshin, D., and Hardy, Lisa, 2009. Re-Os dating of arsenopyrite  
636 from the Galena mine – evidence for Mesoproterozoic age of the Ag-Pb-Zn mineralization in the Coeur  
637 d'Alène district, Idaho. *Geol. Soc. Amer. Annual Meeting*, 18-21 October 2009, Portland, Oregon, USA, 26-1.
- 638 Armstrong, J.T., 1988. Quantitative analysis of silicates and oxide minerals: Comparison of Monte-Carlo, ZAF and  
639 Phi-Rho-Z procedures. *Microb. Anal.* 239-246
- 640 Beziat, D., Monchoux, P., and Tollon, F., 1996. Cobaltite-gersdorffite solid solution as a primary magmatic phase in  
641 spessartite, Lacaune area, Montagne Noire, France. *Can. Miner.* 34, 503-512.

642 Bookstrom, A.A., Johnson, C.A., Landis, G.P., and Frost, T.P., 2007. Blackbird Fe-Cu-Co-Au-REE deposits: U.S.  
643 Geological Survey Open-File Report 2007-1280-B, 13-20, available online at [http://pubs.usgs-  
gov/of/2007/1280](http://pubs.usgs-<br/>644 gov/of/2007/1280)

645 Bookstrom, A.A., 2013. The Idaho cobalt belt. *Northwest Geology* 42, 149-162.

646 Bookstrom, A.A., Box, S.E., Cossette, P.M., Frost, T.P., Gillerman, V.S., King, G.R., and Zirakparvar, N.A., 2016.  
647 Geologic history of the Blackbird Co-Cu district in the Lemhi sub-basin of the Belt-Purcell Basin, in: MacLean,  
648 J.S., and Sears, J.W. (Eds.), *Belt Basin: Window to Mesoproterozoic Earth: Geol. Soc. Amer. Sp. Paper 522*,  
649 available open access on [www.gsapubs.org](http://www.gsapubs.org).

650 Box, S.E., Bookstrom, A.A., and Anderson, R.G., 2012. Origins of mineral deposits, Belt-Purcell Basin, United  
651 States and Canada: An introduction. *Econ. Geol.* 107, 1081-1088.

652 Burmester, R.F., Lonn, J.D., Lewis, R.S., and McFadden, M.D., 2013. Toward a grand unified theory for stratigraphy  
653 of the Lemhi sub-basin of the Belt Supergroup, in: Lewis, R.S., Garsjo, M.M., and Gibson, R.I. (Eds.), *Belt  
654 Symposium V: Missoula, Montana, Tobacco Root Geological Society: Northwest Geol.* 42, 1-19.

655 Connor, J.J., 1991. Some geochemical features of the Blackbird and Jackass Zones of the Yellowjacket Formation  
656 (Middle Proterozoic) in East-Central Idaho. U.S. Geological Survey Open-File Report 91-259A, 25p.

657 Cook, N.J., Ciobanu, C.L., Meria, D., Silcock, D., and Wade, B., 2013. Arsenopyrite-pyrite association in an  
658 orogenic gold ore: Tracing mineralization history from texture and trace elements. *Econ. Geol.* 108, 1273-1283.

659 Creaser, R.A., Papanastassiou, D.A., Wasserburg, G.J., 1991. Negative thermal ion mass spectrometry of osmium,  
660 rhenium and iridium. *Geochim. Cosmochim. Acta* 55, 397-401.

661 Davies, T., Richards, J.P., Creaser, R.A., Heaman, L.M., Chacko, T., Simonetti, A., Williamson, J., and McDonald,  
662 D.W., 2010. Paleoproterozoic age relationships in the Three Bluffs Archean iron formation-hosted gold deposit,  
663 Committee Bay Greenstone Belt, Nunavut, Canada. *Expl. Min. Geol.* 19, 55-80.

664 Donovan, J.J., Snyder, D.A., and Rivers, M.L., 1993. An improved interference correction for trace element analysis.  
665 *Microb. Anal.* 2, 23-28.

- 666 Eiseman, H.H., 1988. Ore geology of the Sunshine cobalt deposit, Blackbird mining district, Idaho (Msc. Thesis):  
667 Golden, Colorado, Colorado School of Mines, 191 p.
- 668 Evans, K.V., 1984. Ordovician plutonism in east-central Idaho: Variation on a Canadian theme. *Geol. Soc. Amer.*  
669 *Abs. Prog.* 16, 504.
- 670 Evans, K.V., and Green, G.N., 2003. Geologic map of the Salmon National Forest and vicinity, east-central Idaho:  
671 U.S. Geological Survey Geologic Investigations Series Map I-2765, 2 sheets, scale 1:100,000, pamphlet, 19 p.
- 672 Evans, K.V., and Zartman, R.E., 1990. U-Th-Pb and Rb-Sr geochronology of Middle Proterozoic granite and augen  
673 gneiss, Salmon River Mountains, east-central Idaho: *Geol. Soc. Amer. Bul.* 102, 63-73.
- 674 Evans, K.V., Aleinikoff, J.N., Obradovich, J.D., and Fanning M.C., 2000. SHRIMP U-Pb geochronology of volcanic  
675 rocks, Belt Supergroup, western Montana: evidence for rapid deposition of sedimentary strata. *Can. J. Earth*  
676 *Sci.* 37, 1287-1300.
- 677 Fleck, R.J., Criss, R.E., Eaton, G.F., Cleland, R.W., Wavra, C.S., and Bond, W.D., 2002. Age and origin of base  
678 and precious metal veins of the Coeur d'Alène mining district, Idaho. *Econ. Geol.* 97, 23-42.
- 679 Foster, D.A., Mueller, P.A., Mogk, D.W., Wooden, J.L., and Vogl, J.J., 2006. Proterozoic evolution of the western  
680 margin of the Wyoming craton: Implications for the tectonic and magmatic evolution of the northern Rocky  
681 Mountains. *Can. J. Earth Sci.* 43, 1601-1619.
- 682 Gasching, R.M., Vervoort, J.D., Lewis, R.S., and McClelland, W.C., 2010. Migrating magmatism in the northern US  
683 cordillera: in situ U-Pb geochronology of the Idaho batholith. *Contrib. Mineral. Petrol.* 159, 863-883.
- 684 Gillerman, V.S., 2008. Geochronology of iron oxide-copper-thorium-REE mineralization in Proterozoic rocks at  
685 Lemhi Pass, Idaho, and a comparison to copper-cobalt ores, Blackbird mining district, Idaho: Final Report to  
686 U.S. Geological Survey, Grant 06HQGR0170, 64 p., with Appendices A to D.
- 687 Hnatyshin, D., Kontak, D.J., Turner, E.C., Creaser, R.A., Morden, R., and Stern, R.A., 2016. Geochronologic (Re-  
688 Os) and fluid-chemical constraints on the formation of the Mesoproterozoic-hosted Nanisivik Zn-Pb deposit,

689 Nunavut, Canada: Evidence for early diagenetic, low-temperature conditions of formation. *Ore Geol. Rev.* 79,  
690 189-217.

691 Huston, D., Wygralak, A., Mernagh, T., Vandenberg, I.C., Crispe, A. J., Lambeck, A., Bagas, L., Cross, A., Fraser,  
692 G., Williams, N., Worden, K., and Meixner, T., 2007. Lode gold mineral systems of the Tanami Region,  
693 northern Australia. *Mineral. Deposita* 42, 175-204.

694 Jiang, S.-Y., Slack, J.F., and Palmer, M.R., 2000. Sm-Nd dating of the giant Sullivan Pb-Zn-Ag deposit, British  
695 Columbia. *Geology* 28, 751-754.

696 Johnson, C.A., Bookstrom, A.A., and Slack, J.F., 2012. Sulfur, carbon, hydrogen, and oxygen isotope geochemistry  
697 of the Idaho cobalt belt. *Econ. Geol.* 107, 1207-1221.

698 Johnson, R., Close, T., and McHugh, E., 1998. Mineral resource appraisal of the Salmon National Forest, Idaho: U.S.  
699 Geological Survey Open-File Report 98-478, p. 277, 7 pl.

700 Kilian, T.M., Chamberlain, K.R., Evans, D.A.D., Bleeker, W., and Cousens, B.L., 2016. Wyoming on the run –  
701 Toward final Paleoproterozoic assembly of Laurentia. *Geology* 44, 863-866.

702 Landis, G.P., and Hofstra, A.H., 2012. Ore genesis constraints on the Idaho cobalt belt from fluid inclusion gas,  
703 noble gas isotope, and ion ratio analyses. *Econ. Geol.* 107, 1189-1205.

704 Lawrence, D.M., Treloar, P.J., Rankin, A.H., Harbidge, P., and Holliday, J., 2013. The geology and mineralogy of  
705 the Loulo mining district, Mali, West Africa: Evidence for two distinct styles of orogenic gold mineralization.  
706 *Econ. Geol.* 108, 199-227.

707 Link, P.K., Fanning, M.C., Lund, K.I., and Aleinikoff, J.N., 2007. Detrital zircon populations and provenance of  
708 Mesoproterozoic strata of east-central Idaho, U.S.A.: Correlation with Belt Supergroup of southwest Montana,  
709 in: Link, P.K., and Lewis, R.L. (Eds.), *Proterozoic geology of western North America and Siberia*. SEPM Sp.  
710 Pub. 86, 101–128.

711 Ludwig, K.R., 2011. User's manual for Isoplot 4.15: A geochronological toolkit for Microsoft Excel.

712 Lund, K., and Tysdal, R.G., 2007. Stratigraphic and structural setting of sediment-hosted Blackbird gold-cobalt-  
713 copper deposits, east-central Idaho, in: Link, P-K., and Lewis, R.L. (Eds.), Proterozoic geology of Western  
714 North America and Siberia: Society for Sedimentary Geology (SPEM) Sp. Pub. 86, 129-147.

715 Lund, K., Aleinikoff, J.N., Evans, K.V., du Bray, E.A., Dewitt, E.H., and Unruh, D.M., 2010, SHRIMP U-Pb dating  
716 of recurrent Cryogenian and Late Cambrian-Early Ordovician alkalic magmatism in central Idaho: implications  
717 for Rodinian rift tectonics: Geological Society of America Bulletin, v. 122, p. 430-453.

718 Lund, K., Tysdal, R.G., Evans, K.V., Kunk, M.J., and Pillers, R.M., 2011. Structural controls and evolution of gold-,  
719 silver-, and REE-bearing copper-cobalt ore deposits, Blackbird district, east-central Idaho — epigenetic origins.  
720 Econ. Geol. 106, 585-618.

721 Mikulski, S. Z., Markey, R. J., and Stein, H. J., 2005. Re-Os ages for auriferous sulfides from the gold deposits in the  
722 Kaczawa Mountains (SW Poland), in: Mineral Deposit Research: Meeting the Global Challenge, Springer  
723 Berlin Heidelberg., pp. 793-796.

724 Morelli, R.M., Bell, C.C., Creaser, R.A., and Simonetti, A., 2010. Constraints on the genesis of gold mineralization  
725 at the Homestake gold deposit, Black Hills, South Dakota from rhenium-osmium sulfide geochronology.  
726 Mineral. Deposita 45, 461-480.

727 Mulder, J., Karlstrom, K., Jacqueline, A., Jones III, J.V., and Holland, M.E., 2016. The Mesoproterozoic sedimentary  
728 record of long-term Australian/Antarctic, Laurentian connections. Geol. Soc. Amer. Annual Meeting, Denver,  
729 Colorado, USA, September 25-28, Abstracts with Programs 48, 7.

730 Nash, J.T., and Connor, J.J., 1993. Iron and chlorine as guides to concordant Cu-Co-Au deposits, Idaho cobalt belt.  
731 Mineral. Deposita 28, 99-106.

732 Nimis, P., Zaykov, V.V., Omenetto, P., Melekestseva, I.Yu, Tesalina, S.G., and Orgeval, J.-J., 2008. Peculiarities of  
733 some mafic-ultramafic- and ultramafic-hosted massive sulfide deposits from the Main Uralian Fault Zone,  
734 southern Urals. Ore Geol. Rev. 33, 49-69.

735 Nold, J.L., 1990. The Idaho cobalt belt, northwestern United States – A metamorphosed Proterozoic exhalative ore  
736 district: Mineral. Deposita 25, 163-168.

737 O'Neill, J.M., 1993. The Great Falls tectonic zone, Montana-Idaho: An Early Proterozoic collisional orogeny  
738 beneath and south of the Belt Basin, in: Berg, R.B. (Ed.), Belt Symposium III, Butte, Montana: Montana  
739 Bureau of Mines and Geology Special Publication 112, 222-228.

740 O'Neil, J.M., Ruppel, E.T., and Lopez, D.A., 2007. Great Divide megashear, Montana, Idaho, and Washington – An  
741 intraplate crustal-scale shear zone recurrently active since the Mesoproterozoic, in: O'Neill, J.M. (Ed.),  
742 Metallogeny of Mesoproterozoic Sedimentary Rocks in Idaho and Montana – Studies by the Mineral Resources  
743 Program, U.S. Geological Survey, 2004-2007. U.S. Geol. Sur. Open-File Rep. 2007-1280-A, 3-10.

744 Panneerselvam, K., MacFarlane, A.W., and Salters, V.J.M., 2012. Reconnaissance lead isotope characteristics of the  
745 Blackbird deposit: Implications for the age and origin of cobalt-copper mineralization in the Idaho cobalt belt,  
746 USA. *Econ. Geol.* 107, 1177-1188.

747 Pitcairn, I.K., Teagle, D.A.H., Craw, D., Olivo, G.R., Kerrich, R., and Brewer, T.S., 2006. Sources of metals and  
748 fluids in orogenic gold deposits: Insights from the Otago and Alpine Schists, New Zealand. *Econ. Geol.* 101,  
749 1525-1546.

750 Pitcairn, I.K., Olivo, G.R., Teagle, D.A.H., and Craw, D., 2010. Sulfide evolution during prograde metamorphism of  
751 the Otago and Alpine Schists, New Zealand. *Can. Mineral.* 48, 1267-1295.

752 Saintilan, N.J., Creaser, R.A., and Spry, P.G., *accepted in Canadian Mineralogist*. Re-Os systematics of löllingite  
753 and arsenopyrite in granulite facies garnet rocks: Insights into the metamorphic evolution of the Broken Hill  
754 block during the Early Mesoproterozoic (New South Wales, Australia)

755 Sims, P.K., O'Neill, J.M., and Bankey, V., 2004. Precambrian basement geologic map of Montana – An  
756 interpretation of aeromagnetic anomalies. U.S. Geol. Sur. Sci. Invest. Map 2829.

757 Slack, J.F., 2006. High REE and Y concentrations in Co-Cu-Au ores of the Blackbird district, Idaho. *Econ. Geol.*  
758 *And Bul. Soc. Econ. Geol.* 101, 275-280.

759 Slack, J.F., 2010. Descriptive and geo-environmental model for Co-Cu-Au deposits in metasedimentary rocks. U.S.  
760 Geological Survey Scientific Investigations Report 2010-5070-G, 218 p.

761 Slack, J.F., 2012. Strata-bound Fe-Co-Cu-Au-Bi-Y-REE deposits of the Idaho Cobalt Belt: Multistage hydrothermal  
762 mineralization in a magmatic-related iron oxide copper-gold system. *Econ. Geol.* 107, 1089-1113.

763 Slack, J.F., 2013. Introduction, chapter 1, in: Slack, J.F. (Ed.), Descriptive and geoenvironmental model for cobalt-  
764 copper-gold deposits, in *Metasedimentary rocks*, chapter G of *Mineral Deposit Models for Resource*  
765 *Assessment* (ver.1.1, March 14, 2014). U.S. Geological Survey Scientific Investigations Report 2010-5070-G,  
766 5-7.

767 Smoliar, M.I., Walker, R.J., Morgan, J.W., 1996, Re-Os ages of Group IIA, IIIA, IVA and IVB iron  
768 meteorites: *Science*, v. 271, p.1099-1102.

769 Stein, H.J., Morgan, J.W., and Scherstén, A., 2000. Re-Os dating of Low-Level Highly Radiogenic (LLHR) sulfides:  
770 The Harnäs gold deposit, southwest Sweden, records continental-scale tectonic events. *Econ. Geol.* 95, 1657-  
771 1671.

772 Trumbull, R.B., Slack, J.F., Krienitz, M.-S., Belkin, H.E., and Wiedenbeck, M., 2011. Fluid sources and  
773 metallogenesis in the Blackbird Co-Cu-Au-Bi-Y-REE district, Idaho, USA: Insights from major element and  
774 boron isotopic compositions of tourmaline. *Can. Miner.* 49, 225-244.

775 Tunks, A., and Cooke, D., 2007. Geological and structural controls on gold mineralization in the Tanami district,  
776 Northern Territory. *Mineral. Deposita* 42, 107-126.

777 Tysdal, R.G., and Desborough, G.A., 1997. Scapolitic metaevaporite and carbonate rocks of Proterozoic  
778 Yellowjacket Formation, Moyer Creek, Salmon River Mountains, central Idaho. U.S. Geological Survey Open-  
779 File Report OF-97-268, 26p.

780 Tysdal, R.G., Lund, K., and Evans, K.V., 2003. Geologic map of the west half of the Salmon National Forest. U.S.  
781 Geological Survey Miscellaneous Investigations Map I-2765, scale 1:100,000.

782 van Acken, D., Su, W., Gao, J., and Creaser, R.A., 2014. Preservation of Re-Os isotope signatures in pyrite  
783 throughout low-T, high-P eclogite facies metamorphism. *Terra Nova* 26, 402-407.

- 784 Vervoort, J.D., Lewis, R.S., Fisher, C., Gasching, R.M., Jansen, A.W., and Brewer, R., 2015. Neoproterozoic and  
785 Paleoproterozoic crystalline basement rocks of north-central Idaho: Constraints on the formation of western  
786 Laurentia. *Geol. Soc. Amer. Bul.* 128, 94-109.
- 787 Vhay, J.S., 1948. Cobalt-copper deposits in the Blackbird district, Lemhi County, Idaho. U.S. Geological Survey  
788 Strategic Minerals Investigation Preliminary Report 3-219, 26 p., 3 pl.
- 789 Völkening, J., Walczyk, T., Heumann, K., 1991. Osmium isotopic ratio determination by negative thermal ionization  
790 mass spectrometry: *Intern. J. Spectro. Ionic Phy.* 105, 147-159.
- 791 Walker, R.J., Morgan, J.W., Naldrett, A.J., Li, C., and Fassett, J.D., 1991. Re-Os isotope systematic of Ni-Cu sulfide  
792 ores, Sudbury Igneous Complex, Ontario: evidence for a major crustal component. *Earth. Pl. Sc. Let.* 105, 416-  
793 429.
- 794 Wang, D., 2015. Age and origin of the Archean and Paleoproterozoic basement rocks from the Priest River and  
795 Clearwater Complexes, Northern Idaho. M.Sc. Thesis, Pullman, Washington, Washington State University, 140  
796 p.
- 797 Winston, D., 1986. Middle Proterozoic tectonics of the Belt Basin, western Montana and northern Idaho, in: Roberts,  
798 S.M. (Ed.), *Belt Supergroup: A guide to Proterozoic rocks of western Montana and adjacent areas.* Montana  
799 Bureau of Mines and Geology Special Publication 94, 245-257.
- 800 Zirakparvar, N.A., Bookstrom, A.A., and Vervoort, J.D., 2007. Cretaceous garnet growth in the Idaho cobalt belt:  
801 Evidence from Lu-Hf geochronology. *Geol. Soc. Amer. Abs. Prog.* 39, 413.
- 802 Zirakparvar, N.A., Vervoort, J.D., McClelland, W., and Lewis, R.S., 2010. Insights into the metamorphic evolution  
803 of the Belt-Purcell basin; evidence from Lu-Hf garnet geochronology. *Can. J. Earth Sci.* 47, 161-179.

804

## 805 **Figure captions**

806 **Fig. 1** Geologic and tectonic maps (modified from Bookstrom and others, 2016), showing the Idaho cobalt belt  
807 (ICB), its geologic surroundings in the Salmon River Mountains, and its regional setting relative to selected tectonic  
808 features. A. Geologic map of the Salmon River Mountains (modified from Evans and Green, 2003) showing the

809 geologic setting of selected Co-Cu-bearing mines, ore zones, and prospects of the ICB, after Johnson and others  
810 (1998). Traces of the iron-oxide zone (OZ) and biotitic Blackbird zone (BZ) after Nash and Connor (1993). Samples  
811 of ore minerals from the Blackbird Chicago (CH) and Idaho (ID) ore zones, the Haynes-Stellite mine (HS), and the  
812 Black Pine prospect (BP) were collected for Re-Os analysis. Names of selected plutons and faults are spelled out, but  
813 names of the following faults are abbreviated as Big Deer fault (BDf), Little Deer fault (LDf), Salmon Canyon fault  
814 (SCf), and White Ledge fault (WLf). B. Tectonic index map (inset) showing the Idaho cobalt belt (ICB) in relation to  
815 the Mesoproterozoic Belt-Purcell basin (Y) and the Lemhi sub-basin (after O'Neill et al., 2007, Box et al., 2012, and  
816 Burmester et al., 2013). Basement domains that surround or project beneath different parts of the Belt-Purcell basin  
817 include the Archean Wyoming Province (A), Medicine Hat block (A), and Paleoproterozoic-Neoproterozoic Clearwater  
818 block (Clwtr blk, XA) after Vervoort et al. (2015), Wang (2015) and Kilian et al. (2016); Paleoproterozoic Selway  
819 terrane (X) after Foster et al. (2006). Major faults of the Great Falls tectonic zone [GFTZ (X) and thrust belt (XA)]  
820 are from O'Neill (1993) and Sims et al. (2004). The Perry line (PL) is a Belt-basin-growth fault (after Winston,  
821 1986). The eastern margin of the East Kootenay Orogen (Y) is drawn to include sites where igneous or metamorphic  
822 minerals yield isotopic age determinations between about 1370 and 1320 Ma. Other features shown include the Great  
823 Divide megashear (GDM, after O'Neill et al., 2007), the rifted continental margin (RCM, after O'Neill et al., 2007),  
824 and accreted oceanic terranes (PzMz = Paleozoic to Mesozoic). Much of the western Belt-Purcell Basin is  
825 overprinted by the metamorphic-plutonic hinterland of the Cordilleran orogen, and its eastern part is overprinted by  
826 the Cordilleran fold-and-thrust belt.

827 **Fig. 2** Simplified columnar stratigraphic section for Mesoproterozoic strata in the Blackbird district (modified after  
828 Bookstrom et al., 2016). The stratigraphic positions of the cobaltite mineralized bodies sampled for Re-Os work are  
829 shown as red ellipses. Blue ellipses correspond to cobaltite mineralized bodies in which U-Pb SHRIMP ages were  
830 produced for xenotime and/or monazite texturally associated with cobaltite (cf. Aleinikoff et al., 2012).

831 **Fig. 3** Highly idealized block diagram representing thrust plates and metamorphic domains in and around the  
832 Blackbird district in the central part of the Idaho Cobalt Belt. Metamorphic grade is illustrated by colored infill.  
833 Approximate locations of the three cobaltite mineralized bodies (CH: Chicago Zone, ID: Idaho Zone, HS: Haynes-  
834 Stellite) sampled for Re-Os geochronology are shown.

835 **Fig. 4** Macrophotographs of the samples processed for Re-Os analyses: a. Haynes-Stellite (HS), b. Chicaco Zone  
836 (CH), c. Idaho Zone (ID), d. Black Pine (BP).

837 **Fig. 5** Complete workflow applied to the samples presented in Figure 4.

838 **Fig. 6** Back-scattered images using a scanning electron microscope of the selected mineral fractions liberated from  
839 each sample following the workflow presented in Figure 5 and mounted in epoxy. Figure 6f is a cobalt distribution  
840 map produced by scanning using an electron microprobe. Abbreviations: CH: Chicago Zone, HS: Haynes-Stellite,  
841 ID: Idaho Zone, BP: Black Pine.

842 **Fig. 7** Graphical representation of the variability of cobalt (Co), iron (Fe), and nickel (Ni) contents determined by  
843 electron microprobe analysis in the various mineral fractions of the samples considered for Re-Os analyses.  
844 Abbreviations: CH: Chicago Zone, HS: Haynes-Stellite, ID: Idaho Zone, BP: Black Pine.

845 **Fig. 8** Conventional Re-Os isochron plot of the analyses of the various magnetic fractions from the Haynes-Stellite  
846 deposit (HS) and the Chicago and Idaho Zones (CH and ID, respectively) in the Blackbird mine. Reference isochrons  
847 with given initial  $^{187}\text{Os}/^{188}\text{Os}$  ratio are shown for reference. Abbreviations: M x.x : Magnetic fraction at current x.x  
848 amps ; NM : x.x : non-magnetic fraction at current x.x amps.

849 **Fig. 9** Diagram of isochron age determination (case 1 with  $n = 7$ , case 2 with  $n = 10$ ) for the Idaho Zone, Blackbird  
850 mine, in the  $^{187}\text{Os}/^{188}\text{Os}$  vs.  $^{187}\text{Re}/^{188}\text{Os}$  space. The empty ellipses represent the 3 data points with high uncertainty.

851 **Fig. 10** Diagram of isochron age determination ( $n = 4$ ) for the Haynes-Stellite deposit in the  $^{187}\text{Os}/^{188}\text{Os}$  vs.  
852  $^{187}\text{Re}/^{188}\text{Os}$  space. The empty ellipses represent the 2 data points with high uncertainty with aliquot size below the  
853 minimum aliquot size of 200 mg.

854 **Fig. 11**  $^{187}\text{Os}/^{188}\text{Os}$  vs.  $1/^{192}\text{Os}$  plot to identify potential mixing relationships.

855 **Fig. 12** Timeline of events for the Belt-Purcell and Lehmi sub-basin. Data after 1: Bookstrom et al., 2016; 2: this  
856 study; 3: Lund et al., 2011; 4: Aleinikoff et al., 2012; 5: Jiang et al, 2001; 6: Aleinikoff et al., 2015; 7: Evans et al.,  
857 2000; 8: Gasching et al., 2010; 9: Anderson and Davies, 1995; 10: Mulder et al., 2016. Abbreviations: BDCG: Big  
858 Deer Creek granite, Fm: Formation.

859

860 **Table labels**

861

862 **Table 1** Blank data for Re-Os analysis. Series « a » and « b » indicate what blank values is appended for each  
863 analysis in Table 2.

864 **Table 2** Statistical summary of electron microprobe analyses and model mineral formula of each variably magnetic  
865 cobaltite fraction in the Chicago Zone and the Idaho Zone in the Blackbird mine, the Haynes-Stellite deposit, and the  
866 Black Pine prospect. ICB : Idaho Cobalt Belt. Abbreviations: M x.x : Magnetic fraction at current x.x amps ; NM :  
867 x.x : non-magnetic fraction at current x.x amps.

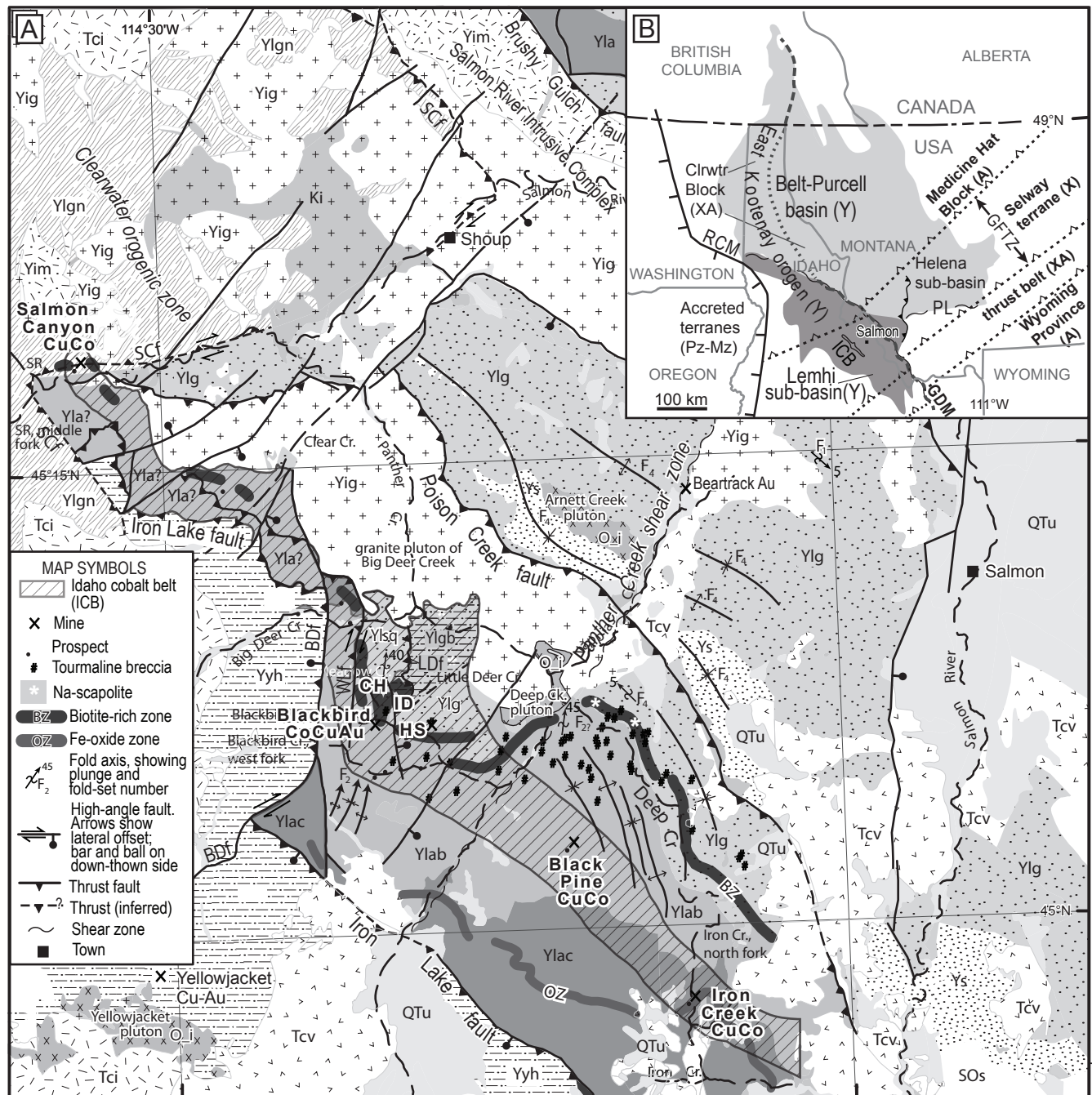
868 **Table 3** Re-Os analytical results for the Chicago Zone and the Idaho Zone in the Blackbird mine, the Haynes-Stellite  
869 deposit, and the Black Pine prospect. Due to low Re levels and high uncertainties in the analyzed Os levels in  
870 cobaltite at the Black Pine prospect, only these values are reported because other items in the Re-Os data set have no  
871 meaning. M x.x: Magnetic fraction at current x.x amps ; NM : x.x : non-magnetic fraction at current x.x amps, side  
872 slope of 15° and forward slope of 10°. Model ages were calculated for aliquots of the Chicago Zone and the Idaho  
873 Zone using an initial  $^{187}\text{Os}/^{188}\text{Os}$  ratio of  $9 \pm 3$  whereas model ages were calculated for aliquots of the Haynes-Stellite  
874 deposit using an initial  $^{187}\text{Os}/^{188}\text{Os}$  ratio of  $5 \pm 2$ .

875

876 **Electronic Supplementary Material**

877

878 **ESM 1.** Full data set of electron microprobe analyses of each variably magnetic cobaltite fraction in the Chicago  
879 Zone and the Idaho Zone in the Blackbird mine, the Haynes-Stellite deposit, and the Black Pine prospect. Detection  
880 limits are: 0.02 wt% for Zn, 0.01 wt% for Fe, 0.03 wt% for Ni, 0.02 wt% for Cu, 0.02 wt% for S, 0.12 wt% for Se,  
881 0.07 wt% for Te, and 0.09 wt% for Bi.



**QUATERNARY-TERTIARY**

- QTu Sediments ± Volcanics, Undivided
- Tci Challis intrusions
- Tcv Challis Volcanics

**CRETACEOUS**

- Ki Granitoid intrusions

**LOWER PALEOZOIC**

- SOs Sedimentary strata (Silurian-Ordovician)
- Oi Syenitoid intrusions (Ordovician-Cambrian, 497 ± 6 Ma)

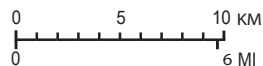
**EXPLANATION OF MAP UNITS**

**MESOPROTEROZOIC**

- Yig Granitic intrusions (1.37 ± 0.01 Ga)
- Yim Mafic intrusions (1.37 ± 0.01 Ga)
- Ys Swauger Fm.

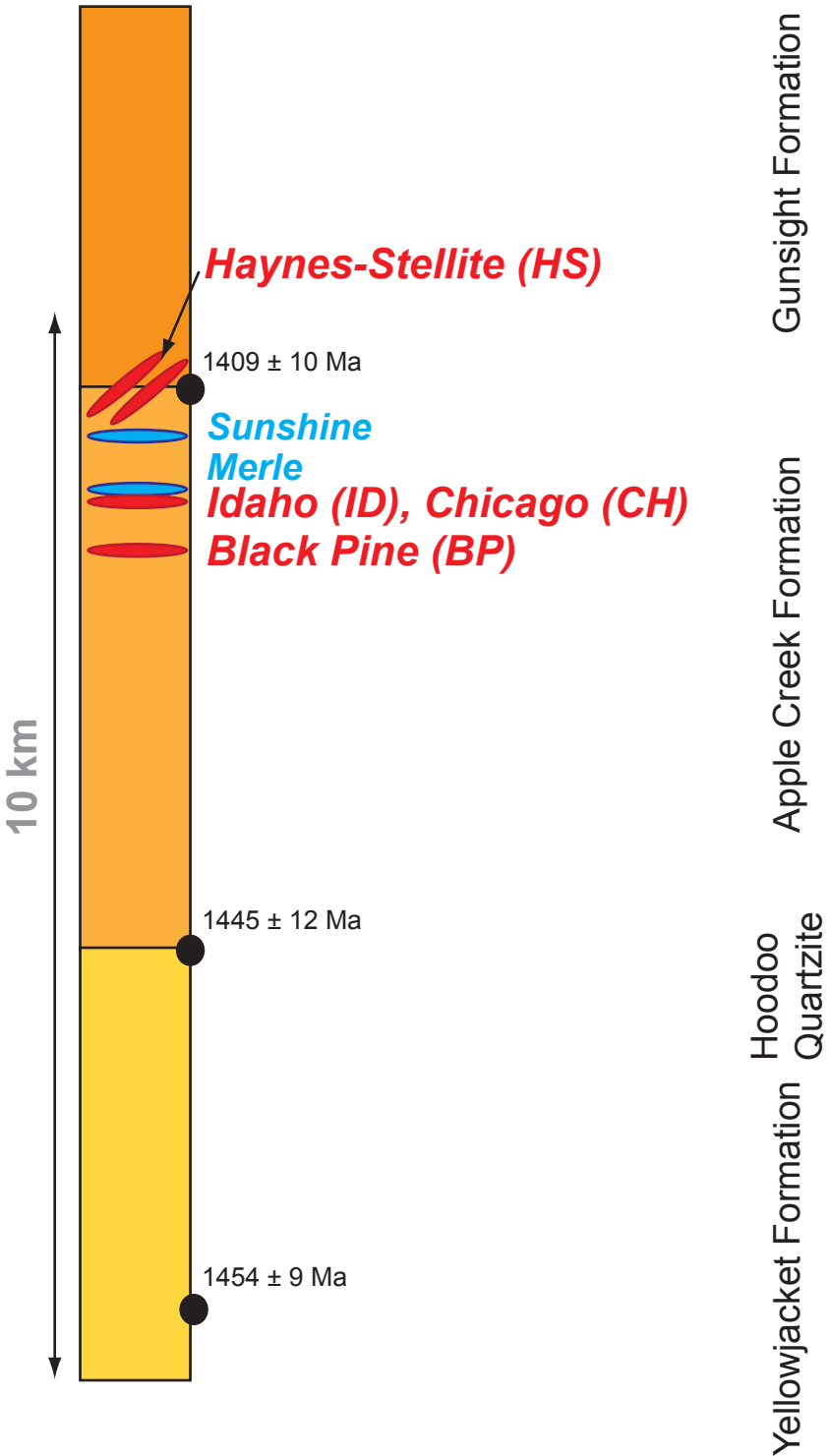
**Lemhi Group**

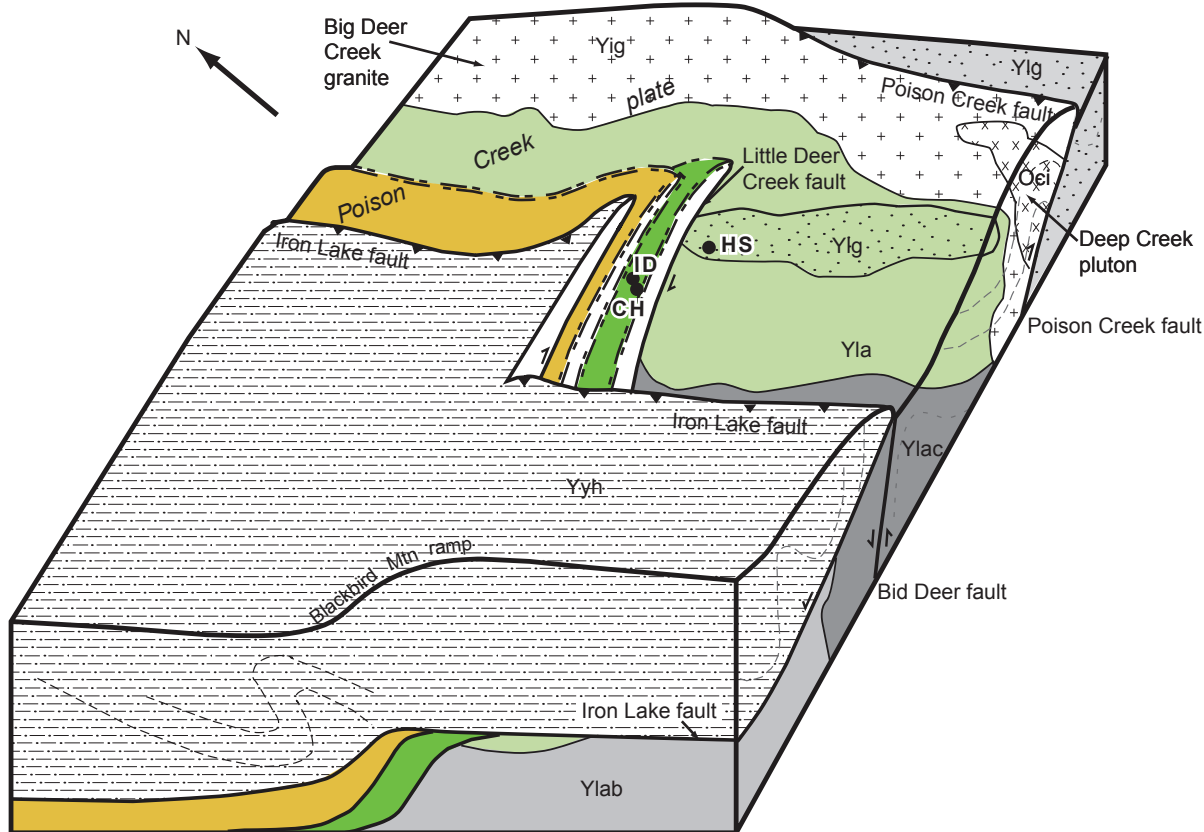
- Ygn Lemhi gneiss (+Grt+Sil)
- Yig Lemhi schist and quartzite
- Yig Gunsight Fm. (Ylg=quartzite facies; Ylgb=biotitic facies)
- Yla Apple Cr. Fm. (of Yellow Lake)
- Ylab Banded siltite unit
- Ylac Coarse siltite unit
- Yyh Yellowjacket and Hoodoo Fms.



# Legend

-  **Black Pine, Idaho, Chicago, Haynes-Stellite** Cobaltite mineralization studied in the present Re-Os work
-  **Sunshine, Merle** Co-Cu mineralization for which geochronology data are available for gangue minerals (xenotime and monazite, *Aleinikoff et al., 2012*)

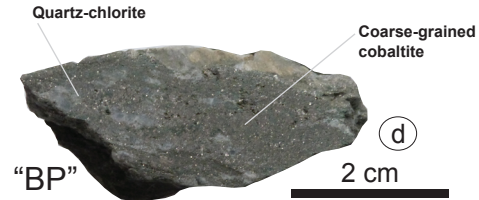
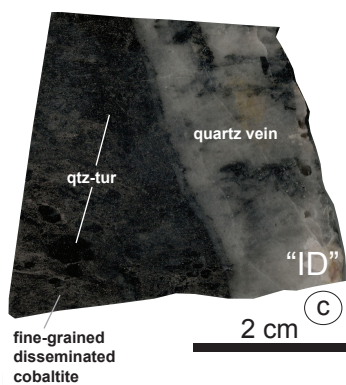
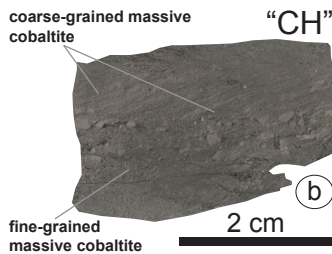


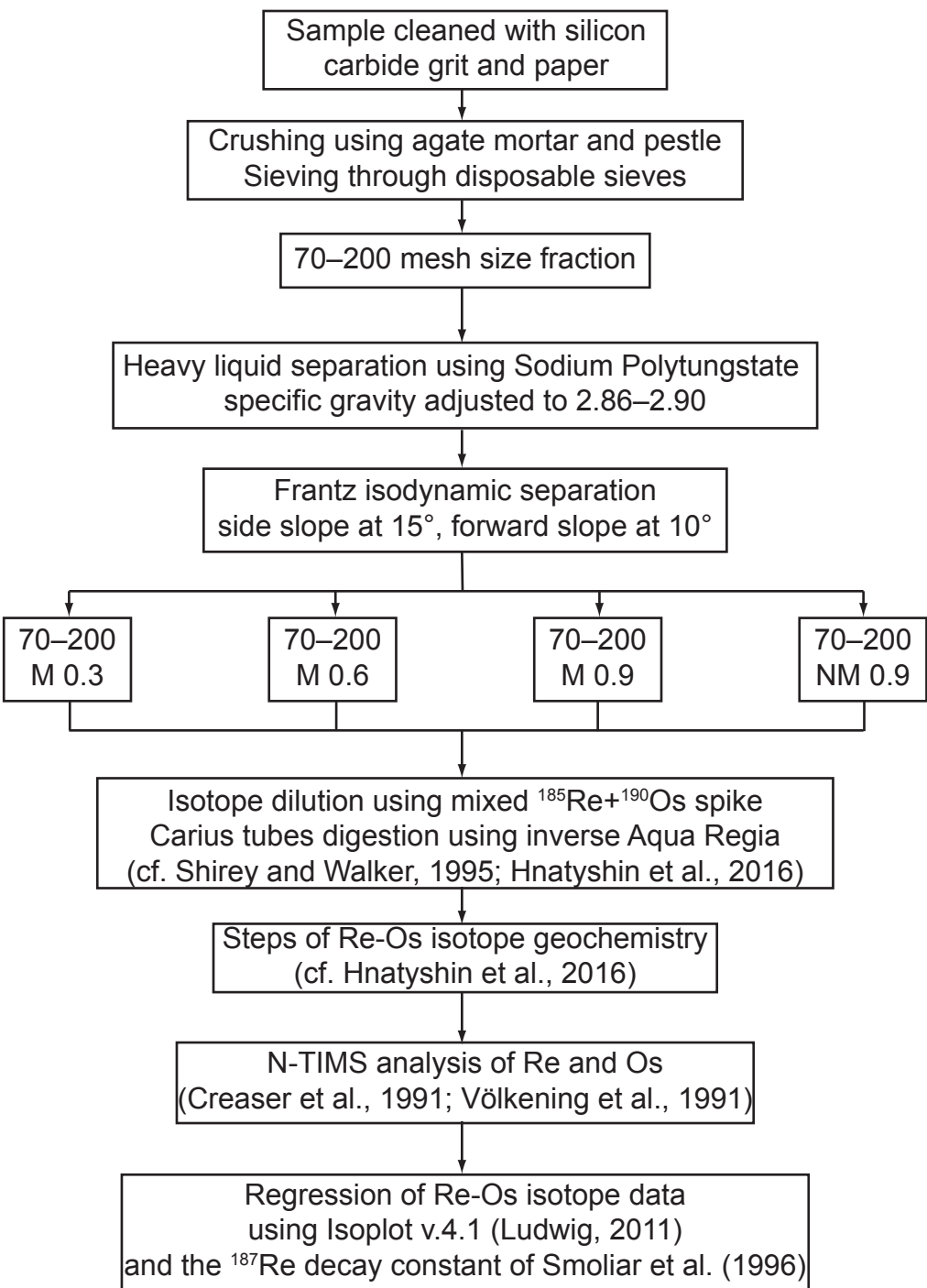


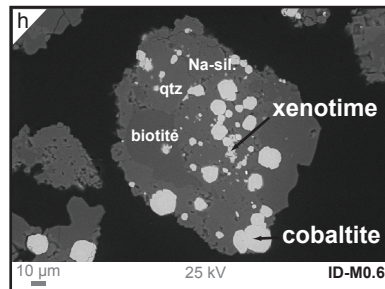
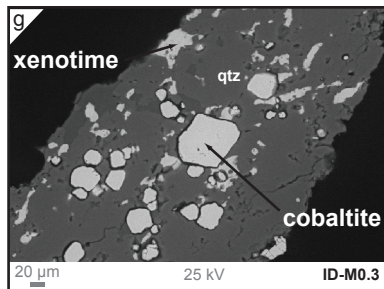
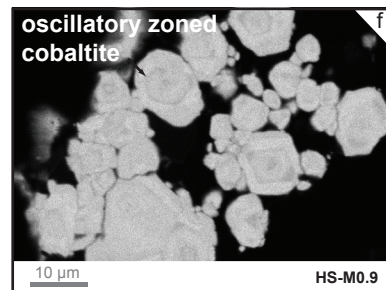
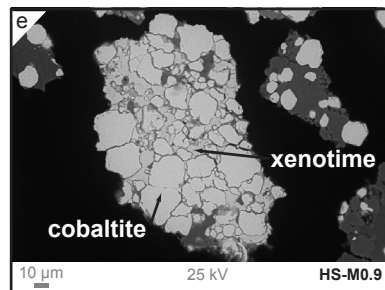
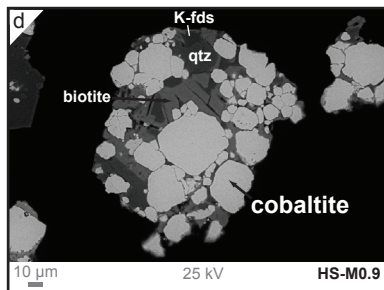
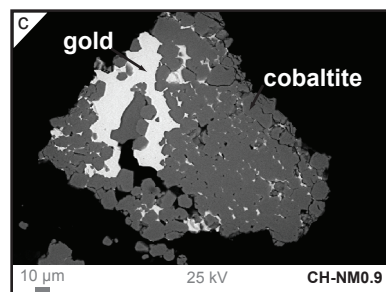
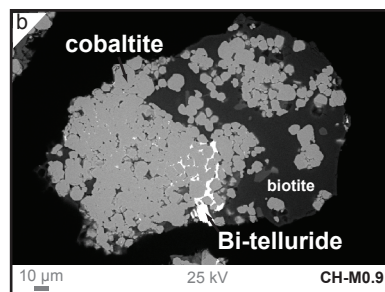
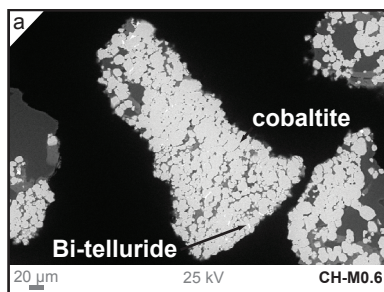
**Indian Creek metamorphic domain**  
 (upper greenschist to lower amphibolite facies, domain containing rocks above garnet isograd)

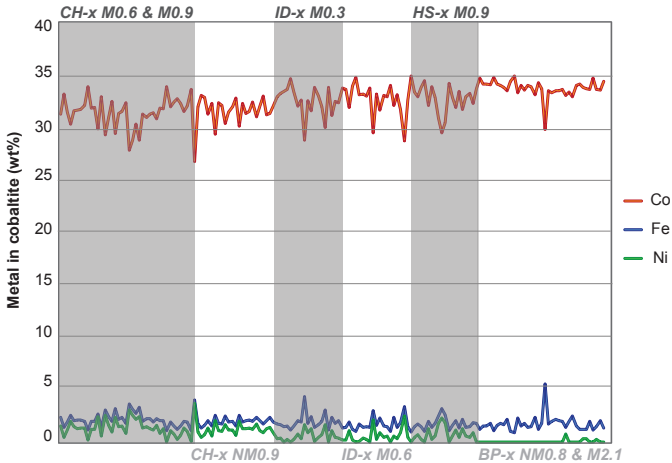
**Blackbird metamorphic domain**  
 (middle to upper greenschist facies)

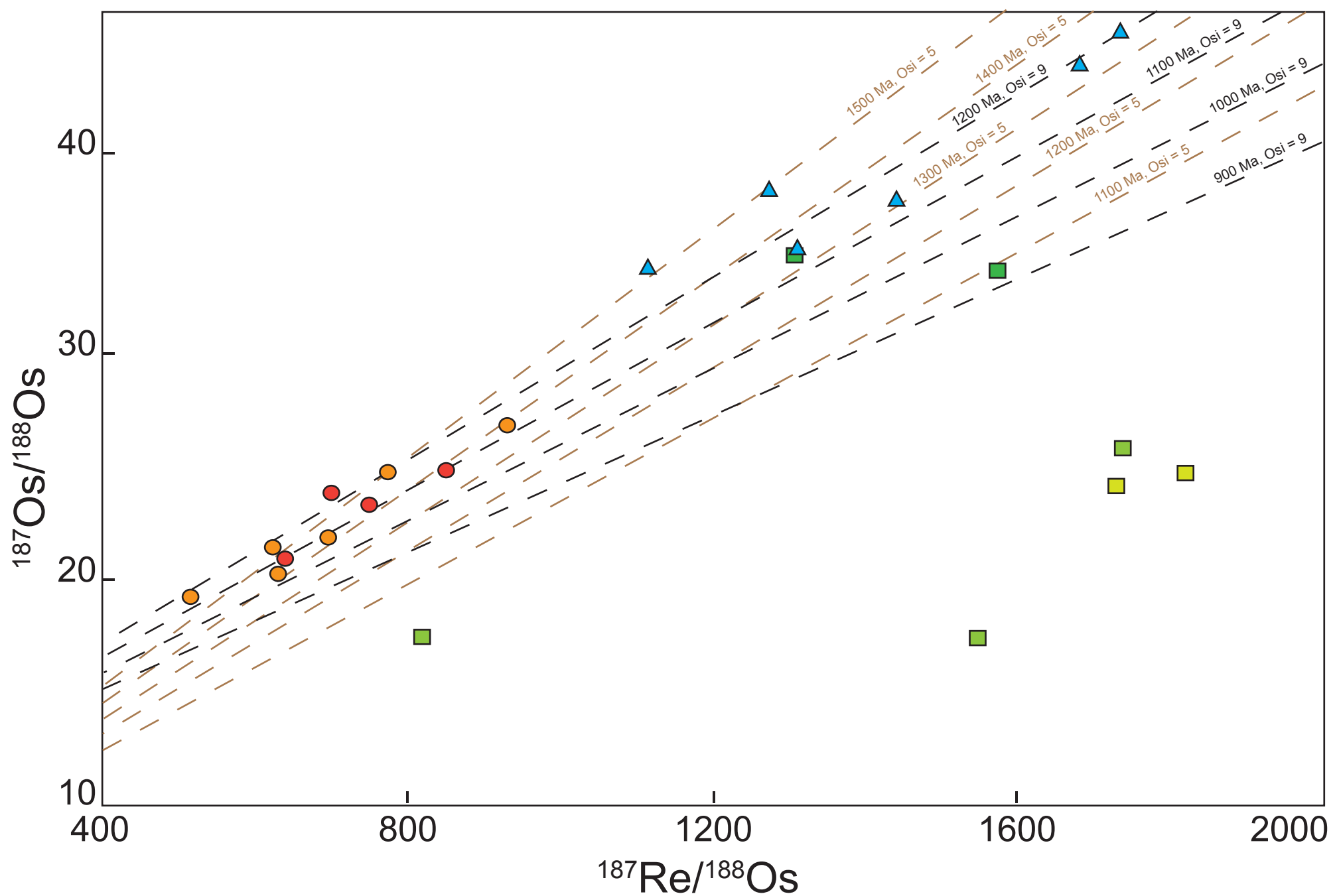
**Haynes-Stellite structural block and metamorphic domain**  
 (lower to middle greenschist facies)





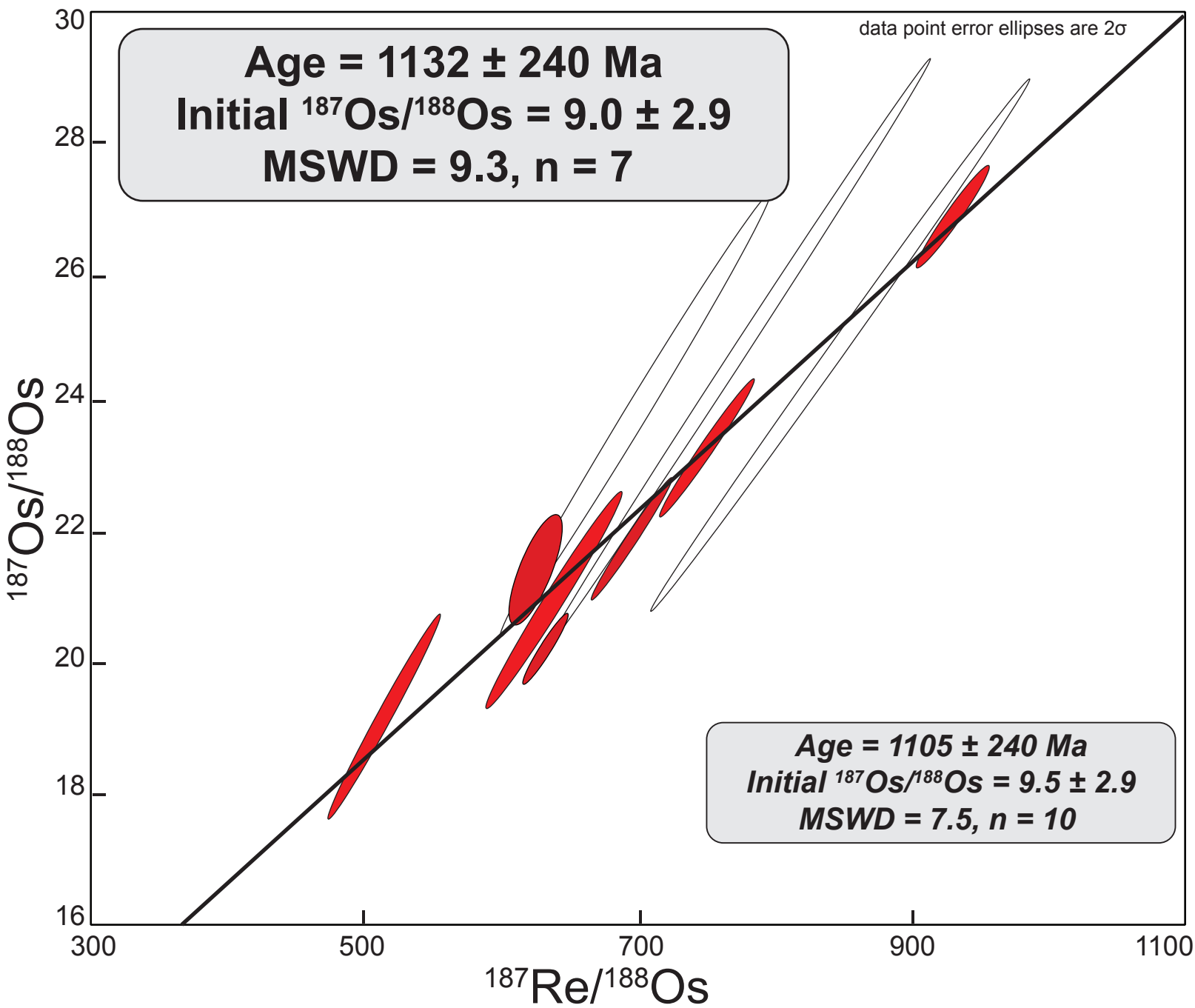


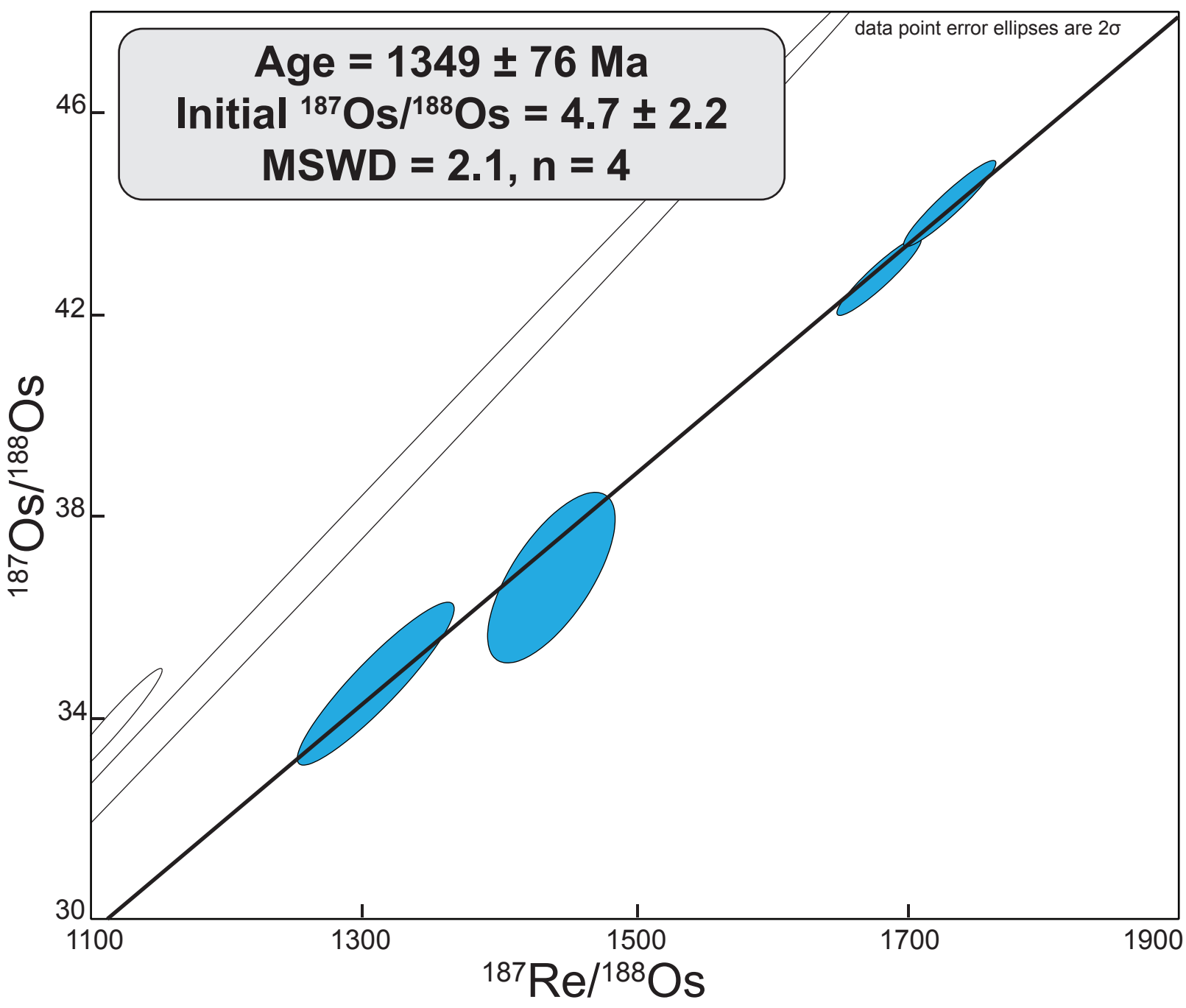


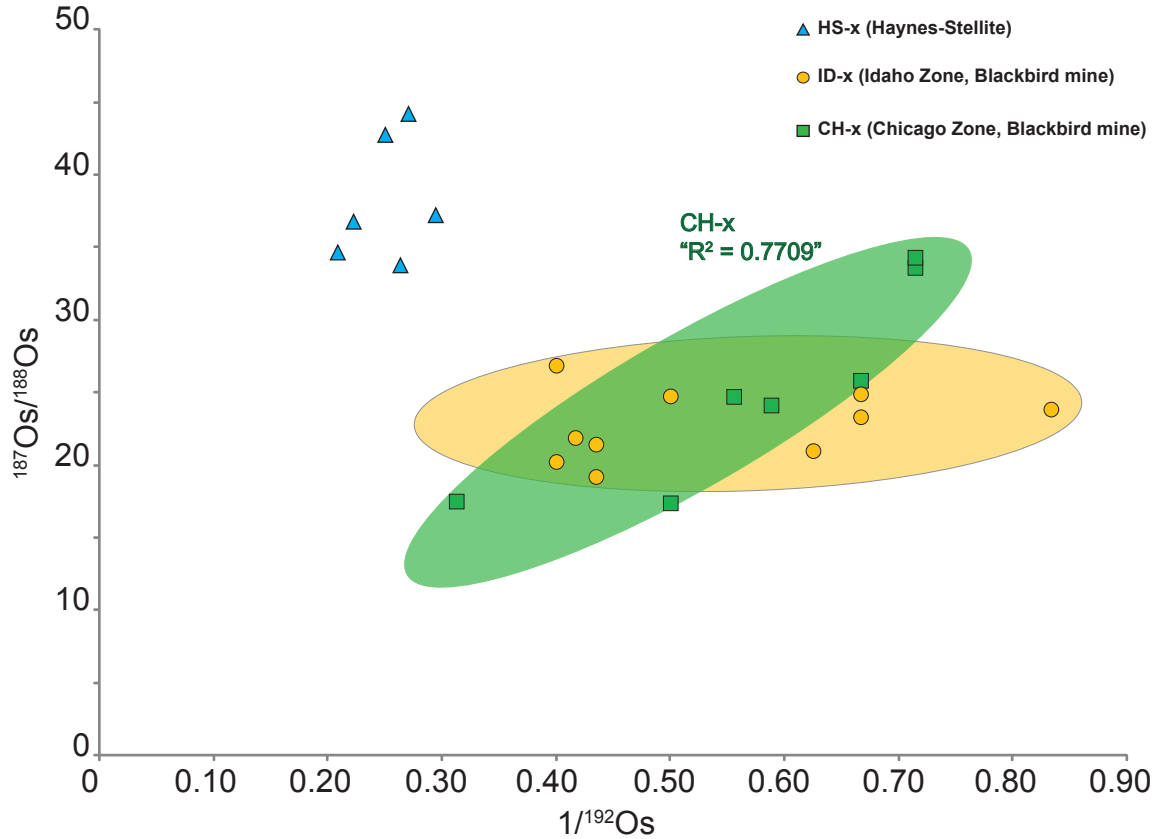


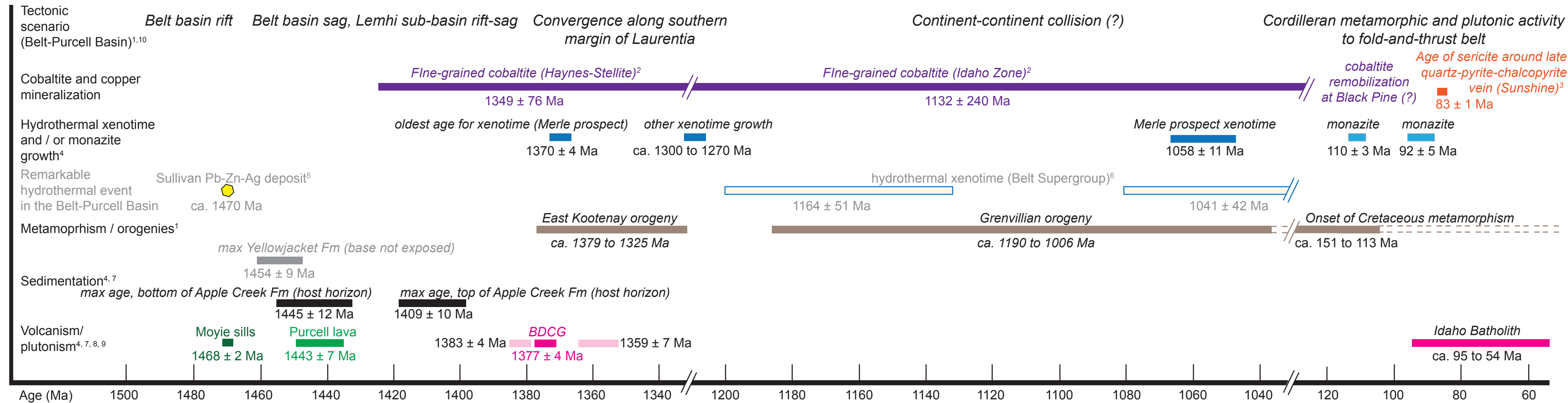
- ▲ HS-x M0.9 (Haynes-Stellite)
- ID-x M0.6 (Idaho Zone, Blackbird mine)
- ID-x M0.3 (Idaho Zone, Blackbird mine)

- CH-x NM0.9 (Chicago Zone, Blackbird mine)
- CH-x M0.9 (Chicago Zone, Blackbird mine)
- CH-x M0.6 (Chicago Zone, Blackbird mine)









<b>Blank series</b>	<b>Blank names</b>	<b>Os blank (pg)</b>	<b>1<math>\sigma</math></b>	<b>Blank <math>^{187}\text{Os} / ^{188}\text{Os}</math></b>	<b>1<math>\sigma</math></b>	<b>Re blank (pg)</b>	<b>1<math>\sigma</math></b>
Series "a", n = 3	BLK-JDH-08, BLK-NS-15Feb16, BLK-NS-23Feb16	1.34	0.03	0.27101	0.0023	4.4	0.98
Series "b", n = 3	BLK-NS-Aug16, BLK-NSEP-1, BLK-NSEP-2	0.08	0.05	0.79623	0.0620	2.3	0.47

Mineral fraction		Zn	Fe	Co	Ni	Cu	S	As	Se	Te	Bi	Modal mineral formula	Metamorphic grade in the structural block	Position in the ICB
		(wt %)												
CH M 0.6 (n = 20)	Min	0.00	1.16	29.49	0.17	0.00	18.50	46.02	0.00	0.00	0.00	$S_{0.97}Fe_{0.06}Co_{0.89}Ni_{0.04}As_{1.03}$	middle to upper greenschist	N W
	Max	0.03	3.21	34.06	2.55	0.00	19.32	46.92	0.00	0.09	0.05			
	average	0.01	2.15	31.72	1.38	0.00	18.81	46.57	0.00	0.02	0.00			
	Standard deviation	0.01	0.51	1.18	0.63	0.00	0.21	0.27	0.00	0.03	0.01			
CH M 0.9 (n = 20)	Min	0.00	1.11	26.91	0.03	0.00	18.78	45.93	0.00	0.00	0.00	$S_{0.98}Fe_{0.07}Co_{0.88}Ni_{0.04}As_{1.03}$	middle to upper greenschist	
	Max	0.03	4.06	34.05	3.70	0.00	19.20	47.03	0.00	0.11	0.20			
	average	0.00	2.20	31.29	1.41	0.00	18.92	46.37	0.00	0.02	0.01			
	Standard deviation	0.01	0.81	1.84	0.96	0.00	0.12	0.30	0.00	0.03	0.04			
CH NM 0.9 (n = 22)	Min	0.00	1.33	29.52	0.47	0.00	18.72	45.35	0.00	0.00	0.00	$S_{0.99}Fe_{0.06}Co_{0.90}Ni_{0.03}As_{1.02}$	middle to upper greenschist	
	Max	0.02	2.58	33.21	2.06	0.00	19.95	46.44	0.36	0.00	0.79			
	average	0.00	1.98	31.91	1.20	0.00	19.10	45.88	0.05	0.00	0.08			
	Standard deviation	0.01	0.52	6.57	0.46	0.00	3.90	9.36	0.08	0.00	0.20			
ID M 0.3 (n = 20)	Min	0.00	1.15	28.93	0.00	0.00	18.83	44.40	0.00	0.00	0.00	$S_{0.99}Fe_{0.06}Co_{0.92}Ni_{0.02}As_{1.01}$	middle to upper greenschist	
	Max	0.01	4.39	34.83	1.65	0.00	19.53	46.67	0.00	0.11	0.03			
	average	0.00	1.96	32.65	0.59	0.00	19.14	45.61	0.00	0.03	0.00			
	Standard deviation	0.00	0.73	1.38	0.51	0.00	0.20	0.55	0.00	0.03	0.01			
ID M 0.6 (n = 20)	Min	0.00	1.01	28.85	0.00	0.00	18.69	44.82	0.00	0.00	0.00	$S_{0.99}Fe_{0.05}Co_{0.93}Ni_{0.02}As_{1.02}$	middle to upper greenschist	
	Max	0.02	3.39	34.99	2.53	0.00	19.59	46.40	0.00	0.07	0.02			
	average	0.01	2.15	31.72	1.38	0.00	18.81	46.57	0.00	0.02	0.00			
	Standard deviation	0.00	0.62	1.48	0.68	0.00	0.22	0.39	0.00	0.03	0.01			
HS M 0.9 (n = 19)	Min	0.00	0.94	29.62	0.00	0.00	18.77	46.27	0.00	0.00	0.00	$S_{0.98}Fe_{0.05}Co_{0.92}Ni_{0.02}As_{1.02}$	lower to middle greenschist	
	Max	0.01	3.19	35.08	2.28	0.00	19.65	46.87	0.00	0.12	0.00			
	average	0.00	1.75	32.90	0.78	0.00	19.11	46.61	0.00	0.03	0.00			
	Standard deviation	0.00	0.56	1.36	0.65	0.00	0.22	0.16	0.00	0.03	0.00			
BP NM 0.8 (n = 18*)	Min	0.00	1.17	30.00	0.00	0.00	18.70	45.69	0.00	0.00	0.00	$S_{0.98}Fe_{0.06}Co_{0.94}Ni_{0.00}As_{1.02}$	lower to middle greenschist	
	Max	0.03	5.57	34.87	0.77	0.01	19.43	46.89	0.00	0.09	0.03			
	average	0.01	1.92	33.63	0.09	0.00	19.10	46.31	0.00	0.02	0.00			
	Standard deviation	0.01	0.99	1.00	0.20	0.00	0.19	0.28	0.00	0.03	0.01			
BP M 2.1 (n = 20)	Min	0.00	0.91	33.28	0.00	0.00	18.69	45.57	0.00	0.00	0.00	$S_{0.98}Fe_{0.05}Co_{0.95}Ni_{0.00}As_{1.02}$	lower to middle greenschist	S E
	Max	0.02	2.36	35.11	0.00	0.00	19.41	46.82	0.00	0.08	0.02			
	average	0.01	1.61	34.19	0.00	0.00	19.04	46.22	0.00	0.02	0.00			
	Standard deviation	0.01	0.40	0.47	0.00	0.00	0.19	0.32	0.00	0.02	0.00			

Sample	Granulometry (mesh size)	Magnetic fraction (15°/10°)	Mineralogy	Sample weight (mg)	Blank series in Table 1	Re		Os		<sup>187</sup> Re/ <sup>188</sup> Os		<sup>187</sup> Os/ <sup>188</sup> Os		rho	<sup>192</sup> Os		<sup>187</sup> Re		<sup>187</sup> Os*		% <sup>187</sup> Os*	%Re blank	% <sup>187</sup> Os blank	% <sup>188</sup> Os blank	Model age <sup>1</sup>		
						± 2σ	± 2σ	± 2σ	± 2σ	± 2σ	± 2σ	± 2σ	± 2σ		± 2σ	± 2σ	± 2σ	± 2σ	± 2σ	± 2σ					± 2σ	± 2σ	
BP-01	+70	M0.8	cobaltite ± chlorite ± quartz	109.70	a	0.295	0.004	3.5	11.3	-	-	-	-	-	(ppt)	(ppb)	(ppt)										
BP-02	+70	NM0.8	cobaltite ± chlorite ± quartz	71.40	a	0.135	0.005	0.8	4.0	-	-	-	-	-													
BP-03	70-200	M1.9	cobaltite ± chlorite ± quartz	36.00	a	<0.100	0.010	-	-	-	-	-	-	-													
BP-04	70-200	M2.1	cobaltite ± chlorite ± quartz	96.30	a	0.117	0.004	0.2	1.9	-	-	-	-	-													
CH-01	70-200	NM0.9	cobaltite ± xenotime ± quartz	77.40	a	1.127	0.008	18.6	9.5	1571	696	33.63	14.90	0.999	1.4	0.708	0.005	10.6	3	57	5.05	3.96	83	934	274		
CH-02	70-200	M0.9	cobaltite ± xenotime ± quartz	53.90	a	1.574	0.011	16.0	7.2	1545	692	17.40	7.80	0.999	2.0	0.990	0.007	4.7	4	30	5.19	7.74	83	326	280		
CH-03	70-200	M0.6	cobaltite ± xenotime ± quartz ± biotite	93.58	a	1.626	0.009	18.1	5.8	1818	532	24.74	7.25	0.999	1.8	1.022	0.006	8.3	3	46	2.89	3.57	77	517	216		
CH-04	70-200	M0.6	cobaltite ± xenotime ± quartz ± biotite	351.90	a	1.500	0.008	17.3	1.5	1729	139	24.15	1.94	0.997	1.7	0.943	0.005	7.7	2	45	0.83	1.00	47	524	209		
CH-05	70-200	M0.9	cobaltite ± xenotime ± quartz	427.09	a	1.336	0.007	16.1	1.3	1736	130	25.85	1.93	0.996	1.5	0.839	0.004	7.7	2	47	0.77	0.87	45	580	208		
CH-06	70-200	NM0.9	cobaltite ± xenotime ± quartz	545.87	a	0.925	0.005	18.7	1.8	1304	101	34.33	3.08	0.859	1.4	0.581	0.003	10.8	2	58	0.87	0.56	41	1155	285		
CH-07	70-200	M0.9	cobaltite ± xenotime ± quartz	349.85	a	1.319	0.007	25.4	1.9	817	56	17.52	1.40	0.853	3.2	0.829	0.004	7.6	4	30	0.95	0.75	33	623	444		
HS-01	70-200	M0.9	cobaltite ± tourmaline ± xenotime ± biotite ± K-feldspar ± quartz	51.57	a	2.186	0.013	48.4	15.8	1273	352	37.26	10.31	0.999	3.4	1.374	0.008	29.4	5	61	3.90	2.24	76	1503	198		
HS-02	70-200	M0.9	cobaltite ± tourmaline ± xenotime ± biotite ± K-feldspar ± quartz	311.90	a	3.131	0.016	63.5	2.7	1309	47	34.69	1.32	0.920	4.8	1.968	0.010	37.1	6	58	0.45	0.29	27	1346	183		
HS-03	70-200	M0.9	cobaltite ± tourmaline ± xenotime ± biotite ± K-feldspar ± quartz	205.30	b	3.258	0.014	63.1	2.4	1438	38	36.82	1.39	0.688	4.5	2.048	0.009	38.2	6	60	0.34	0.07	3	1313	170		
HS-04	70-200	M0.9	cobaltite ± tourmaline ± xenotime ± biotite ± K-feldspar ± quartz	266.37	b	3.398	0.014	64.0	1.1	1680	25	42.80	0.63	0.932	4.0	2.136	0.009	41.7	5	65	0.25	0.05	3	1336	142		
HS-05	70-200	M0.9	cobaltite ± tourmaline ± xenotime ± biotite ± K-feldspar ± quartz	145.75	b	2.106	0.009	49.1	1.6	1114	31	33.8	1.0	0.971	3.8	1.323	0.006	28.3	5	58	0.75	0.13	5	1533	213		
HS-06	70-200	M0.9	cobaltite ± tourmaline ± xenotime ± biotite ± K-feldspar ± quartz	268.79	b	3.202	0.013	60.2	1.2	1732	28	44.24	0.71	0.941	3.7	2.012	0.008	39.8	5	66	0.27	0.06	3	1345	137		
ID-01	70-200	M0.3	cobaltite ± biotite ± xenotime	158.90	a	0.791	0.005	20.8	3.4	771	116	24.77	3.72	0.999	2.0	0.497	0.003	9.5	3	46	3.50	1.83	63	1216	474		
ID-02	70-200	M0.6	cobaltite ± biotite ± quartz ± xenotime	238.60	a	0.650	0.004	15.7	2.3	847	113	24.9	3.3	0.999	1.5	0.497	0.002	7.2	2	46	2.84	1.62	60	1117	430		
ID-03	70-200	M0.3	cobaltite ± biotite ± xenotime	100.86	b	0.589	0.004	19.3	1.3	512	34	19.22	1.28	0.989	2.3	0.370	0.003	6.7	3	34	3.87	0.55	12	1186	700		
ID-04	70-200	M0.3	cobaltite ± biotite ± xenotime	332.57	b	0.729	0.003	21.4	0.6	622	16	21.45	0.69	0.759	2.3	0.458	0.002	8.4	3	40	0.95	0.15	4	1190	575		
ID-05	70-200	M0.6	cobaltite ± biotite ± quartz ± xenotime	107.94	b	0.425	0.004	12.0	1.5	697	81	23.87	2.78	0.995	1.2	0.267	0.002	5.3	2	44	5.01	0.77	19	1267	519		
ID-06	70-200	M0.6	cobaltite ± biotite ± quartz ± xenotime	267.67	b	0.578	0.003	15.0	0.6	749	28	23.33	0.87	0.985	1.5	0.364	0.002	6.5	2	43	1.49	0.25	7	1138	477		
ID-07	70-200	M0.3	cobaltite ± biotite ± xenotime	260.97	b	1.154	0.005	26.9	0.7	929	22	26.89	0.65	0.969	2.5	0.725	0.003	13.2	3	49	0.76	0.14	4	1145	384		
ID-08	70-200	M0.6	cobaltite ± biotite ± quartz ± xenotime	150.03	b	0.511	0.003	14.4	1.0	637	41	21.00	1.35	0.986	1.6	0.321	0.002	5.5	2	39	3.00	0.48	11	1121	563		
ID-09	70-200	M0.3	cobaltite ± biotite ± xenotime	288.17	b	0.794	0.003	22.0	0.5	630	14	20.26	0.44	0.954	2.5	0.499	0.002	8.1	3	37	1.00	0.17	4	1063	567		
ID-10	70-200	M0.3	cobaltite ± biotite ± xenotime	182.00	b	0.840	0.004	22.4	0.8	695	24	21.91	0.77	0.986	2.4	0.528	0.002	16.6	0	74	1.50	0.25	7	1105	514		

Sample	Zn wt%	Fe wt%	Co wt%	Ni wt%	Cu wt%	S wt%
01-CZ-M06_001	0.00	2.36	31.44	1.53	0.00	18.87
01-CZ-M06_002	0.01	1.39	33.37	0.46	0.00	19.00
01-CZ-M06_003	0.00	1.95	31.63	1.16	0.00	18.86
01-CZ-M06_004	0.00	2.54	30.49	1.99	0.00	18.60
01-CZ-M06_005	0.00	2.07	31.76	1.45	0.00	18.67
01-CZ-M06_006	0.00	2.14	31.80	1.28	0.00	18.85
01-CZ-M06_007	0.00	2.11	31.86	1.38	0.00	19.04
01-CZ-M06_008	0.01	2.02	32.25	1.38	0.00	19.00
01-CZ-M06_009	0.00	1.16	34.06	0.17	0.00	19.32
01-CZ-M06_010	0.01	1.99	31.99	1.21	0.00	18.53
01-CZ-M06_011	0.00	2.01	32.10	1.20	0.00	18.62
01-CZ-M06_012	0.01	2.69	30.01	2.45	0.00	18.59
01-CZ-M06_013	0.00	1.38	33.10	0.61	0.00	19.02
01-CZ-M06_014	0.03	3.07	29.49	2.55	0.00	18.50
01-CZ-M06_015	0.02	2.44	31.13	1.58	0.00	18.80
01-CZ-M06_016	0.00	2.02	32.63	1.00	0.00	18.79
01-CZ-M06_017	0.00	3.21	29.58	2.38	0.00	18.60
01-CZ-M06_018	0.01	2.19	31.51	1.48	0.00	18.67
01-CZ-M06_019	0.00	2.39	31.67	1.51	0.00	18.89
01-CZ-M06_020	0.01	1.82	32.52	0.83	0.00	18.98
01-CZ-M09_001	0.00	3.63	27.97	3.09	0.00	18.84
01-CZ-M09_002	0.01	3.17	28.97	2.54	0.00	19.02
01-CZ-M09_003	0.00	2.74	30.51	2.16	0.00	18.78
01-CZ-M09_004	0.00	3.33	28.92	2.41	0.00	18.85
01-CZ-M09_005	0.03	1.98	31.44	1.36	0.00	18.79
01-CZ-M09_006	0.01	2.26	31.10	1.46	0.00	18.91
01-CZ-M09_007	0.01	2.23	31.46	1.28	0.00	19.03
01-CZ-M09_008	0.00	1.92	31.54	1.14	0.00	18.80
01-CZ-M09_009R	0.01	2.24	31.02	1.63	0.00	18.97
01-CZ-M09_010	0.00	2.06	32.01	0.82	0.00	19.08
01-CZ-M09_011	0.01	2.06	31.97	1.28	0.00	18.92
01-CZ-M09_012	0.00	1.11	34.05	0.03	0.00	19.20
01-CZ-M09_013	0.00	1.91	32.15	1.10	0.00	18.78
01-CZ-M09_014	0.01	1.57	32.60	0.75	0.00	19.01
01-CZ-M09_015R	0.00	1.24	32.92	0.29	0.00	19.04
01-CZ-M09_016	0.00	1.51	32.49	0.64	0.00	18.80
01-CZ-M09_017	0.01	2.02	31.73	1.36	0.00	18.83
01-CZ-M09_018	0.00	1.91	32.20	1.04	0.00	18.92
01-CZ-M09_019	0.00	1.11	33.81	0.05	0.00	19.07
01-CZ-M09_020	0.00	4.06	26.91	3.70	0.00	18.80
01-CZ-NM09_001	0.00	1.73	32.17	1.00	0.00	18.97
01-CZ-NM09_002	0.01	1.33	33.21	0.47	0.00	19.82
01-CZ-NM09_003	0.01	1.58	33.01	0.71	0.00	19.15
01-CZ-NM09_004R	0.01	2.07	31.43	1.32	0.00	19.12
01-CZ-NM09_005	0.00	1.56	32.49	0.59	0.00	19.18
01-CZ-NM09_006R	0.01	2.58	29.52	2.06	0.00	18.82

01-CZ-NM09_007	0.00	1.78	32.54	1.11	0.00	19.22
01-CZ-NM09_008R	0.01	1.74	32.28	1.04	0.00	18.98
01-CZ-NM09_009	0.00	2.50	30.51	1.64	0.00	19.04
01-CZ-NM09_010	0.02	1.94	31.63	1.17	0.00	18.91
01-CZ-NM09_011	0.00	1.96	32.14	1.14	0.00	19.95
01-CZ-NM09_012Rb	0.00	1.55	32.97	0.65	0.00	18.98
01-CZ-NM09_013R	0.00	2.56	30.28	1.96	0.00	18.90
01-CZ-NM09_014R	0.00	1.93	32.47	1.26	0.00	19.26
01-CZ-NM09_015R	0.00	2.08	31.53	1.29	0.00	18.83
01-CZ-NM09_016	0.00	2.10	31.71	1.34	0.00	18.99
01-CZ-NM09_017	0.00	1.97	32.57	1.22	0.00	19.03
01-CZ-NM09_018	0.00	2.39	31.19	1.73	0.00	19.01
01-CZ-NM09_019	0.01	2.03	32.21	1.08	0.00	19.09
01-CZ-NM09_020	0.00	1.75	33.16	0.87	0.00	19.18
01-CZ-NM09_021	0.02	2.06	31.40	1.31	0.00	18.72
01-CZ-NM09_022	0.00	2.37	31.51	1.40	0.00	19.00
01-IZ-M0.3_001	0.00	1.95	32.22	0.89	0.00	18.83
01-IZ-M0.3_002	0.00	1.70	33.12	0.34	0.00	19.18
01-IZ-M0.3_003	0.00	1.67	33.41	0.36	0.00	19.18
01-IZ-M0.3_004	0.00	1.49	33.64	0.00	0.00	19.40
01-IZ-M0.3_005	0.00	1.52	33.84	0.29	0.00	19.20
01-IZ-M0.3_006	0.00	1.15	34.83	0.00	0.00	19.53
01-IZ-M0.3_007	0.01	1.57	33.54	0.27	0.00	19.08
01-IZ-M0.3_008	0.00	2.06	32.20	0.77	0.00	19.12
01-IZ-M0.3_009	0.00	1.90	32.80	0.34	0.00	19.23
01-IZ-M0.3_010	0.00	4.39	28.93	1.65	0.00	19.09
01-IZ-M0.3_011	0.01	1.78	32.72	0.89	0.00	18.84
01-IZ-M0.3_012	0.00	2.42	31.77	1.26	0.00	19.15
01-IZ-M0.3_013	0.00	1.41	33.99	0.06	0.00	19.46
01-IZ-M0.3_014	0.00	1.66	33.19	0.47	0.00	19.00
01-IZ-M0.3_015	0.01	2.00	32.17	0.73	0.00	19.06
01-IZ-M0.3_016	0.00	3.11	30.16	1.64	0.00	18.84
01-IZ-M0.3_017	0.00	1.19	34.03	0.00	0.00	19.40
01-IZ-M0.3_018	0.00	2.41	31.30	1.11	0.00	19.14
01-IZ-M0.3_019	0.00	1.79	32.68	0.44	0.00	19.19
01-IZ-M0.3_020	0.00	2.06	32.53	0.38	0.00	18.97
01-IZ-M0.6_001	0.00	1.35	33.95	0.21	0.00	19.14
01-IZ-M0.6_002	0.01	1.43	33.81	0.22	0.00	19.19
01-IZ-M0.6_003R	0.00	1.95	32.10	1.06	0.00	18.95
01-IZ-M0.6_004	0.00	1.24	34.12	0.19	0.00	19.48
01-IZ-M0.6_005	0.00	1.03	34.99	0.00	0.00	19.59
01-IZ-M0.6_006	0.00	1.73	33.30	0.09	0.00	19.36
01-IZ-M0.6_007	0.00	1.39	33.36	0.36	0.00	19.08
01-IZ-M0.6_008	0.00	1.50	33.15	0.28	0.00	19.06
01-IZ-M0.6_009	0.00	1.42	33.91	0.00	0.00	19.23
01-IZ-M0.6_010	0.01	3.04	29.64	2.15	0.00	19.00
01-IZ-M0.6_011	0.00	1.61	33.36	0.28	0.00	18.92

01-IZ-M0.6_012	0.00	2.30	31.84	0.88	0.00	19.03
01-IZ-M0.6_013	0.00	1.54	33.21	0.43	0.00	19.04
01-IZ-M0.6_014	0.00	1.46	33.11	0.57	0.00	19.00
01-IZ-M0.6_015	0.00	1.01	34.21	0.00	0.00	19.28
01-IZ-M0.6_016	0.02	2.37	32.25	0.58	0.00	18.97
01-IZ-M0.6_017	0.01	1.39	33.32	0.32	0.00	19.06
01-IZ-M0.6_018	0.00	1.86	31.86	0.87	0.00	18.69
01-IZ-M0.6_019	0.00	3.39	28.85	2.53	0.00	18.83
01-IZ-M0.6_020	0.00	1.46	32.79	0.48	0.00	18.90
HS-01-M09_001	0.00	0.94	35.08	0.00	0.00	19.23
HS-01-M09_003	0.01	1.45	33.53	0.43	0.00	19.30
HS-01-M09_004	0.01	1.72	33.09	0.71	0.00	19.31
HS-01-M09_005	0.00	1.49	33.97	0.24	0.00	19.65
HS-01-M09_006	0.00	1.01	34.65	0.00	0.00	19.31
HS-01-M09_007	0.00	1.97	32.28	1.30	0.00	19.33
HS-01-M09_008	0.00	1.44	34.09	0.24	0.00	19.12
HS-01-M09_009	0.00	1.81	33.07	0.57	0.00	19.13
HS-01-M09_010	0.00	2.49	31.09	1.77	0.00	19.00
HS-01-M09_011	0.00	3.19	29.62	2.28	0.00	18.79
HS-01-M09_012	0.00	2.61	30.63	1.89	0.00	18.77
HS-01-M09_013	0.01	1.08	34.36	0.02	0.00	19.34
HS-01-M09_014	0.01	1.62	33.02	0.60	0.00	19.03
HS-01-M09_015	0.00	2.07	32.10	1.14	0.00	19.06
HS-01-M09_016	0.00	1.34	33.59	0.43	0.00	19.04
HS-01-M09_017	0.00	2.16	31.88	1.26	0.00	18.90
HS-01-M09_018	0.00	1.44	33.10	0.59	0.00	18.95
HS-01-M09_019	0.00	1.51	33.42	0.44	0.00	18.86
HS-01-M09_020	0.00	1.86	32.43	0.93	0.00	18.96
NS-02-BP M2.1_001	0.00	1.82	33.89	0.00	0.00	18.86
NS-02-BP M2.1_002	0.00	1.22	34.88	0.00	0.00	19.26
NS-02-BP M2.1_003	0.01	1.53	34.33	0.00	0.00	19.25
NS-02-BP M2.1_004	0.00	1.57	34.34	0.00	0.00	19.06
NS-02-BP M2.1_005	0.01	1.78	34.24	0.00	0.00	18.89
NS-02-BP M2.1_006	0.00	1.10	34.93	0.00	0.00	19.34
NS-02-BP M2.1_007	0.01	1.64	34.32	0.00	0.00	19.04
NS-02-BP M2.1_008	0.01	1.82	34.21	0.00	0.00	18.99
NS-02-BP M2.1_009	0.00	1.64	34.03	0.00	0.00	19.11
NS-02-BP M2.1_010	0.01	2.20	33.67	0.00	0.00	19.22
NS-02-BP M2.1_011	0.01	1.03	34.60	0.00	0.00	19.05
NS-02-BP M2.1_012	0.00	0.91	35.11	0.00	0.00	19.41
NS-02-BP M2.1_013	0.00	2.33	33.47	0.00	0.00	18.92
NS-02-BP M2.1_014	0.01	1.55	34.21	0.00	0.00	19.01
NS-02-BP M2.1_015	0.01	1.82	33.74	0.00	0.00	19.11
NS-02-BP M2.1_016	0.01	1.41	34.17	0.00	0.00	19.00
NS-02-BP M2.1_017	0.02	1.48	34.07	0.00	0.00	18.69
NS-02-BP M2.1_018	0.01	2.36	33.28	0.00	0.00	18.90
NS-02-BP M2.1_019	0.00	1.21	34.42	0.00	0.00	18.92

NS-02-BP M2.1_020	0.00	1.79	33.89	0.00	0.00	18.79
NS-02-BP NM0.8_003	0.02	5.57	30.00	0.00	0.00	18.84
NS-02-BP NM0.8_004	0.03	1.72	33.66	0.03	0.00	19.11
NS-02-BP NM0.8_005	0.01	2.01	33.51	0.00	0.00	19.12
NS-02-BP NM0.8_006	0.00	2.17	33.65	0.00	0.00	18.99
NS-02-BP NM0.8_007	0.00	2.04	33.66	0.00	0.00	19.06
NS-02-BP NM0.8_008	0.00	1.98	33.82	0.00	0.00	19.11
NS-02-BP NM0.8_009	0.00	1.42	33.20	0.77	0.00	19.29
NS-02-BP NM0.8_010	0.00	2.00	33.55	0.00	0.00	19.08
NS-02-BP NM0.8_011	0.00	2.48	33.11	0.00	0.00	19.09
NS-02-BP NM0.8_012	0.01	1.55	34.20	0.00	0.00	19.04
NS-02-BP NM0.8_013	0.02	1.21	34.31	0.00	0.00	18.90
NS-02-BP NM0.8_014	0.00	1.24	33.97	0.30	0.00	19.27
NS-02-BP NM0.8_015	0.00	1.21	33.90	0.35	0.00	19.27
NS-02-BP NM0.8_016	0.01	2.02	33.81	0.00	0.00	18.89
NS-02-BP NM0.8_017	0.00	1.17	34.87	0.00	0.01	18.70
NS-02-BP NM0.8_018	0.00	1.47	33.78	0.23	0.00	19.34
NS-02-BP NM0.8_019	0.00	2.03	33.76	0.00	0.00	19.25
NS-02-BP NM0.8_020	0.01	1.34	34.58	0.00	0.00	19.43

---

<b>As wt%</b>	<b>Se wt%</b>	<b>Te wt%</b>	<b>Bi wt%</b>	<b>Total</b>
46.54	0.00	0.00	0.00	100.75
46.31	0.00	0.06	0.00	100.60
46.83	0.00	0.03	0.00	100.47
46.73	0.00	0.02	0.00	100.37
46.89	0.00	0.00	0.05	100.89
46.53	0.00	0.01	0.00	100.62
46.63	0.00	0.02	0.00	101.03
46.58	0.00	0.00	0.00	101.24
46.12	0.00	0.09	0.00	100.92
46.79	0.00	0.00	0.00	100.53
46.53	0.00	0.03	0.00	100.48
46.28	0.00	0.00	0.00	100.02
46.22	0.00	0.00	0.00	100.31
46.72	0.00	0.01	0.00	100.37
46.84	0.00	0.00	0.03	100.83
46.47	0.00	0.05	0.00	100.95
46.91	0.00	0.04	0.00	100.72
46.92	0.00	0.00	0.00	100.77
46.64	0.00	0.00	0.00	101.10
46.02	0.00	0.05	0.00	100.23
46.29	0.00	0.03	0.00	99.84
46.45	0.00	0.00	0.00	100.15
46.91	0.00	0.00	0.00	101.10
47.03	0.00	0.03	0.00	100.58
46.62	0.00	0.00	0.20	100.41
46.65	0.00	0.00	0.00	100.39
46.49	0.00	0.00	0.00	100.49
45.93	0.00	0.02	0.00	99.35
46.04	0.00	0.00	0.00	99.91
46.01	0.00	0.00	0.00	99.98
46.53	0.00	0.00	0.00	100.78
46.31	0.00	0.00	0.00	100.70
46.50	0.00	0.11	0.00	100.56
46.44	0.00	0.02	0.00	100.39
45.93	0.00	0.04	0.00	99.46
46.15	0.00	0.00	0.00	99.59
46.31	0.00	0.02	0.00	100.27
46.39	0.00	0.03	0.00	100.48
46.14	0.00	0.02	0.00	100.20
46.33	0.00	0.05	0.00	99.85
45.63	0.00	0.36	0.79	100.66
45.50	0.00	0.14	0.56	101.04
45.99	0.00	0.02	0.00	100.47
45.66	0.00	0.01	0.00	99.62
45.89	0.00	0.03	0.00	99.75
45.35	0.00	0.04	0.00	98.38

46.09	0.00	0.05	0.00	100.80
45.87	0.00	0.03	0.00	99.94
45.91	0.00	0.00	0.02	99.63
45.44	0.00	0.00	0.01	99.11
45.78	0.00	0.04	0.04	101.06
46.11	0.00	0.01	0.00	100.28
46.32	0.00	0.00	0.00	100.04
46.05	0.00	0.00	0.00	100.97
46.05	0.00	0.00	0.00	99.77
46.16	0.00	0.00	0.00	100.29
46.44	0.00	0.02	0.00	101.23
46.41	0.00	0.06	0.00	100.78
46.00	0.00	0.04	0.01	100.46
45.58	0.00	0.01	0.00	100.54
45.71	0.00	0.11	0.25	99.58
45.50	0.00	0.05	0.00	99.82
46.13	0.00	0.02	0.00	100.04
45.33	0.00	0.00	0.00	99.67
45.55	0.00	0.11	0.00	100.28
45.12	0.00	0.07	0.03	99.75
46.27	0.00	0.00	0.00	101.13
45.15	0.00	0.00	0.00	100.66
45.62	0.00	0.03	0.00	100.13
45.61	0.00	0.00	0.00	99.76
45.67	0.00	0.00	0.00	99.94
46.29	0.00	0.01	0.00	100.35
46.67	0.00	0.05	0.00	100.97
46.11	0.00	0.01	0.00	100.72
45.97	0.00	0.03	0.00	100.92
45.54	0.00	0.03	0.00	99.89
45.63	0.00	0.05	0.00	99.65
44.74	0.00	0.03	0.00	98.52
44.40	0.00	0.05	0.00	99.08
45.49	0.00	0.03	0.00	99.48
45.05	0.00	0.05	0.00	99.19
45.83	0.00	0.00	0.00	99.77
46.19	0.00	0.00	0.00	100.83
46.32	0.00	0.01	0.00	100.98
46.40	0.00	0.04	0.00	100.50
46.06	0.00	0.07	0.00	101.16
45.56	0.00	0.07	0.00	101.23
44.82	0.00	0.00	0.00	99.30
45.96	0.00	0.03	0.00	100.18
45.41	0.00	0.06	0.00	99.46
45.49	0.00	0.00	0.00	100.05
46.15	0.00	0.07	0.00	100.06
45.70	0.00	0.00	0.00	99.87

45.54	0.00	0.05	0.00	99.64
45.77	0.00	0.06	0.00	100.04
46.02	0.00	0.01	0.01	100.17
45.26	0.00	0.06	0.00	99.82
45.95	0.00	0.00	0.00	100.14
45.95	0.00	0.07	0.00	100.12
45.50	0.00	0.03	0.00	98.82
45.69	0.00	0.00	0.02	99.32
45.57	0.00	0.00	0.00	99.20
46.27	0.00	0.09	0.00	101.61
46.76	0.00	0.06	0.00	101.55
46.87	0.00	0.02	0.00	101.74
46.45	0.00	0.02	0.00	101.82
46.44	0.00	0.00	0.00	101.41
46.68	0.00	0.00	0.00	101.57
46.61	0.00	0.04	0.00	101.54
46.64	0.00	0.00	0.00	101.22
46.87	0.00	0.01	0.00	101.23
46.72	0.00	0.04	0.00	100.64
46.77	0.00	0.08	0.00	100.73
46.35	0.00	0.12	0.00	101.27
46.43	0.00	0.00	0.00	100.71
46.49	0.00	0.04	0.00	100.91
46.57	0.00	0.00	0.00	100.98
46.67	0.00	0.04	0.00	100.92
46.57	0.00	0.03	0.00	100.68
46.60	0.00	0.00	0.00	100.83
46.75	0.00	0.05	0.00	101.00
46.60	0.00	0.01	0.00	101.18
46.19	0.00	0.06	0.00	101.61
46.37	0.00	0.00	0.00	101.49
46.52	0.00	0.03	0.00	101.50
46.64	0.00	0.00	0.00	101.55
46.31	0.00	0.04	0.02	101.75
46.82	0.00	0.00	0.00	101.84
46.58	0.00	0.00	0.00	101.62
46.38	0.00	0.03	0.00	101.20
46.31	0.00	0.02	0.00	101.42
46.08	0.00	0.00	0.00	100.77
45.57	0.00	0.01	0.00	101.01
46.12	0.00	0.08	0.00	100.92
46.07	0.00	0.01	0.00	100.86
45.71	0.00	0.00	0.00	100.40
46.03	0.00	0.04	0.00	100.66
45.97	0.00	0.04	0.00	100.26
46.07	0.00	0.00	0.00	100.63
45.90	0.00	0.01	0.00	100.47

46.17	0.00	0.00	0.00	100.65
45.69	0.00	0.00	0.00	100.11
46.36	0.00	0.09	0.00	101.01
46.60	0.00	0.00	0.00	101.25
46.57	0.00	0.01	0.00	101.39
46.54	0.00	0.00	0.00	101.30
46.26	0.00	0.00	0.00	101.18
46.04	0.00	0.00	0.00	100.71
46.49	0.00	0.02	0.00	101.13
46.36	0.00	0.06	0.00	101.11
46.30	0.00	0.01	0.03	101.14
46.14	0.00	0.00	0.00	100.57
45.94	0.00	0.00	0.00	100.72
46.06	0.00	0.00	0.00	100.81
46.14	0.00	0.07	0.00	100.93
46.89	0.00	0.00	0.00	101.63
46.39	0.00	0.01	0.00	101.23
46.50	0.00	0.04	0.00	101.57
46.23	0.00	0.02	0.00	101.61

---

## Highlights

1. Variably magnetic fractions of cobaltite in the ICB have low Re and total Os contents (ca. 0.4–4 ppb and 14–64 ppt, respectively) but elevated  $^{187}\text{Re}/^{188}\text{Os}$  (600–1800) and highly radiogenic  $^{187}\text{Os}/^{188}\text{Os}$  (17–45) ratios. The Black Pine prospect has too low Re concentrations ( $<0.3$  ppb) to produce any reliable Re-Os data. By contrast, Re-Os data of cobaltite from the quartz-tourmaline-cobaltite breccia Haynes-Stellite deposit are accurate and reproducible providing a minimum aliquot size of 200 mg whereas data for cobaltite from the quartz-tourmaline-cobaltite breccia of the Idaho Zone require a minimum aliquot size of 150 mg.
2. The Re-Os systematics in cobaltite at Haynes-Stellite and at the Idaho Zone are preserved and Re-Os data are regressed using the isochron approach. By contrast, the Re-Os systematics of cobaltite in the Chicago Zone are disturbed and a linear array of mixing with post-depositional hydrothermal fluids is identified in the  $^{187}\text{Os}/^{188}\text{Os}$  vs.  $1/^{192}\text{Os}$  space. Cobaltite was primarily deposited in the ICB at Haynes Stellite at  $1349 \pm 76$  Ma and was preceded by REE-Y-mineral precipitation at ca. 1370 Ma in connection with the emplacement of the Big Deer Creek granite at ca. 1377 Ma as part of a suite of bimodal magmatic activity between ca. 1383 and 1359 Ma (Aleinikoff et al., 2012). We propose that our age of  $1132 \pm 240$  Ma for cobaltite in the quartz-tourmaline breccia in the Idaho Zone and consideration of other geologic and structural constraints (Bookstrom et al., 2007, 2016) illustrate a remobilization phase of pre-existing cobaltite mineralization along cleavages and folds during the 1190–1006 Ma Grenvillian orogeny.
3. Cobaltite formed at ca. 1349 Ma upon cooling at an inferred temperature of  $\leq 300^\circ\text{C}$  of a mixture of Mesoproterozoic evaporitic brines and magmatic fluids that carried both metals and reduced sulfur. The extremely high initial Os ratio derived from regression of the Re-Os data at Haynes-Stellite ( $4.7 \pm 2.2$ ) is used as a tracing tool to identify the source of metals. The most likely scenario considers that metals were derived from lower crustal mafic source rocks of probable Archean age, overlain by oceanic island-arc rocks of Paleoproterozoic age, which are tectonically interlayered with Archean rocks of the Wyoming Province continental nucleus, in the collisional

Great Falls tectonic zone, which projects beneath the Idaho Cobalt Belt. This scenario is compatible with the sulfur isotopic composition of cobaltite ( $+8.0 \pm 0.4\text{‰}$ ) that is best explained by reduced sulfur being sourced from deep, crustal and highly metamorphosed rocks (Johnson et al., 2012).

4. We propose that the Re-Os isotope system in cobaltite in the Chicago Zone, located in a middle greenschist facies metamorphic zone, may have been subjected to temperatures of 400 to 520°C proposed for Cretaceous garnet-bearing rocks of a lower amphibolites facies metamorphic domain above the domain hosting the Chicago Zone. A maximum closing temperature of 400°C is inferred for Re-Os in cobaltite. By contrast, cobaltite at Haynes-Stellite and the Idaho Zone, which underwent middle to lower greenschist Cretaceous metamorphism, preserved Mesoproterozoic age information delivered by the Re-Os isotope system.